Environmental Science and Pollution Research (2024) 31:21986–22011
https://doi.org/10.1007/s11356-024-32262-9

RESEARCH ARTICLE

The research on a novel multivariate grey model and its application in carbon dioxide emissions prediction

Yan Xu[1,2] · Tong Lin[1] · Pei Du[3,4] · Jianzhou Wang[5]

Received: 29 September 2023 / Accepted: 26 January 2024 / Published online: 24 February 2024

Abstract

Accurate small-sample prediction is an urgent, very difficult, and challenging task due to the quality of data storage restricted in most realistic situations, especially in developing countries. The grey model performs well in small-sample prediction. Therefore, a novel multivariate grey model is proposed in this study, called FBNGM (1, N, r), with a fractional order operator, which can increase the impact of new information and background value coefficient to achieve high prediction accuracy. The utilization of an intelligence optimization algorithm to tune the parameters of the multivariate grey model is an improvement over the conventional method, as it leads to superior accuracy. This study conducts two sets of numerical experiments on CO_2 emissions to evaluate the effectiveness of the proposed FBNGM (1, N, r) model. The FBNGM (1, N, r) model has been shown through experiments to effectively leverage all available data and avoid the problem of overfitting. Moreover, it can not only obtain higher prediction accuracy than comparison models but also further confirm the indispensable importance of various influencing factors in CO_2 emissions prediction. Additionally, the proposed FBNGM (1, N, r) model is employed to forecast CO_2 emissions in the future, which can be taken as a reference for relevant departments to formulate policies.

Keywords Carbon emission forecasting · Multivariate grey models · Fractional order operator · Intelligence optimization algorithm

Introduction

Background

In recent years, climate warming has emerged as one of the most significant environmental challenges faced by countries worldwide. The continuous rise in carbon dioxide (CO_2) emissions is considered a major contributor to increased greenhouse gas emissions and subsequent global warming (Li et al. 2022). Global CO_2 emissions have experienced a sharp increase over the past few decades, nearly doubling to alarming levels, as reported by the International Energy Agency (IEA) (Ding and Zhang 2023). This surge is primarily attributed to the combustion of fossil fuels such as coal, oil, and natural gas to meet energy demands and industrial production (Liu et al. 2022). Consequently, the international community has increasingly recognized the importance of reducing CO_2 emissions and addressing climate change. Under the Paris Agreement, which aims to contain the increase in global average temperature to below 2 °C above pre-industrial levels and strives to limit warming to 1.5 °C to reduce the impact of climate change on the ecosystem, the economy, and human societies, each country sets its emission reduction targets and adopts corresponding emission reduction measures (Ding and Zhang 2023).

According to the World Bank, the top three emitters in terms of CO_2 emissions in 2020 are China (109,446,686.2 kT), the USA (43,205,532.5 kT), and India (22,008,360.3 kT) (as shown in Fig. 1). Only three of the top 10 countries in terms of CO_2 emissions are below the world average in

Responsible Editor: Marcus Schulz

✉ Pei Du
dupeijnu@yeah.net

[1] Ocean University of China, Qingdao 266100, China

[2] Qingdao Financial Research Institute, Qingdao 266100, China

[3] School of Business, Jiangnan University, Wuxi 214122, China

[4] Food Safety Research Base of Jiangsu Province, Jiangnan University, Wuxi 214122, China

[5] Institute of Systems Engineering, Macau University of Science and Technology, Macau 999078, China

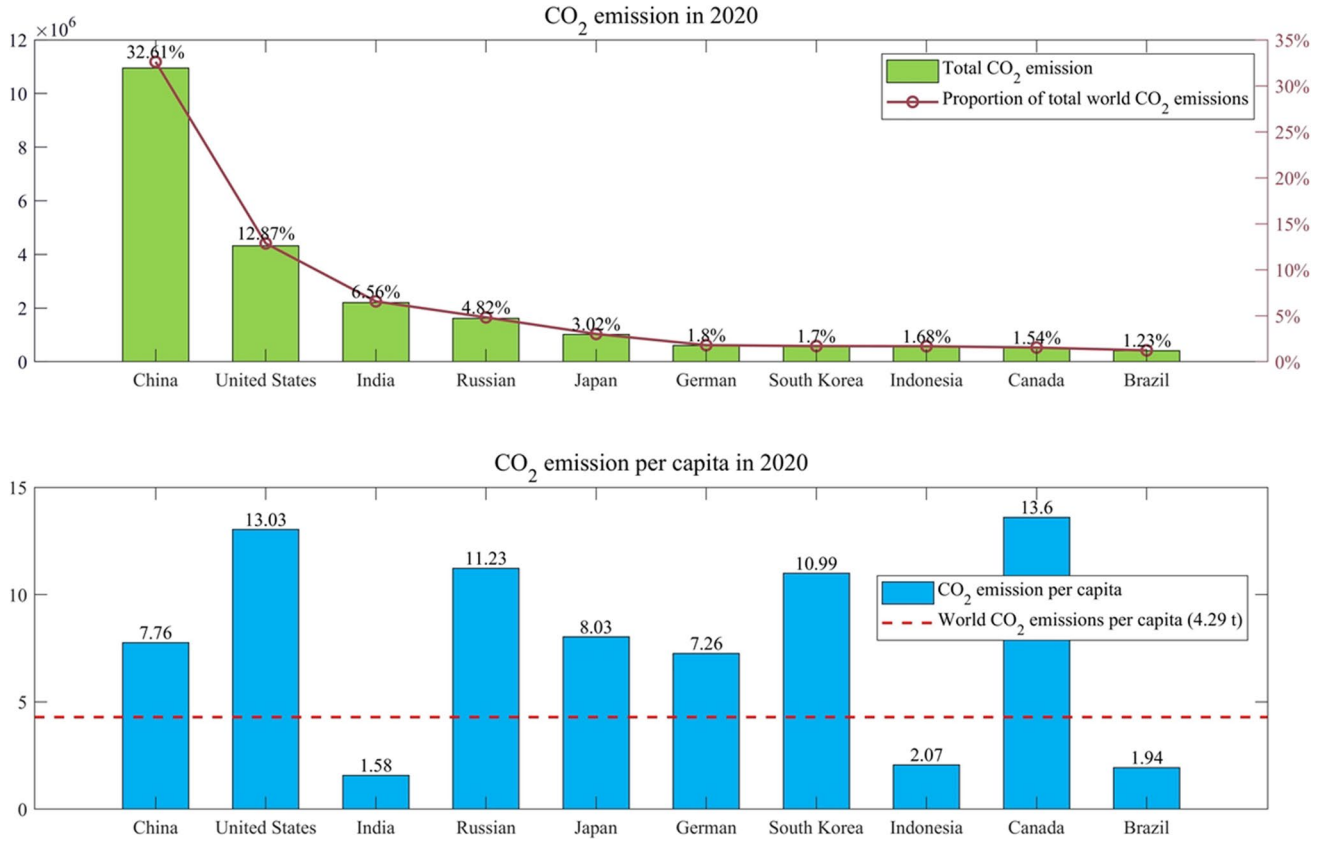

Fig. 1 CO_2 emissions in 2020

terms of CO_2 emissions per capita, with Canada (13.6 T) ranking first among these 10 countries. Statistically, China accounts for 32.6% of global CO_2 emissions, ranking first in the world. As the world's largest carbon emitter, China is committed to making efforts to reduce global carbon emissions, and in the general debate of the 75th session of the United Nations General Assembly, China explicitly proposed that it would strive to achieve the goal of "carbon peaking" by 2030 and "carbon neutrality" by 2060 (Wei et al. 2023).

Subsequently, China has taken a series of measures to accelerate the realization of the "dual-carbon" goal (Ding et al. 2023a). To promote the adoption of low-carbon technologies and sustainable practices among enterprises, China has set up the world's largest carbon trading market, which provides economic incentives and benefits to businesses (Zeraibi et al. 2022). In addition, China is promoting the transformation of its energy structure (He et al. 2022), phasing out highly polluting and energy-consuming traditional energy industries and increasing the proportion of renewable energy (Xin-Gang et al. 2022). However, China, being a developing country, continues to grapple with the significant challenge of striking a balance between rapid economic growth and reducing carbon emissions (Huang et al. 2022a; Li et al. 2021a). As the economy expands, the environment faces mounting pressures, and the contradiction between sustainable development and carbon emission reduction becomes increasingly pronounced (Wang et al. 2021; Umar et al. 2021). Consequently, it becomes crucial to accurately predict CO_2 emissions to aid decision-makers in promptly responding to climate change, adjusting existing energy-saving and emission-reduction policies, and formulating feasible programs to promote low-carbon sustainable development (Ye et al. 2022).

To respond to climate change and environmental pollution promptly, it is necessary to accurately predict CO_2 emissions by taking into account a combination of factors. However, due to the small amount of data for some factors, the current popular big data methods are not applicable, so there is an urgent need for a small-sample prediction method to cope with this situation.

As a result, this study proposes a fractional-order multivariate grey prediction model with optimized background values that can accurately predict CO_2 emissions per capita,especially because the model effectively integrates numerous relevant influencing factors and obtains the highest accuracy in both cases. The superior prediction accuracy of the model is attributed to the ability of the fractional-order cumulative operator to make full use of the new

information and the optimization of the background value coefficient, which can be used to obtain accurate and stable prediction results. Therefore, the model can be used to predict future CO_2 emission projections per capita, thus providing a reliable basis for policymakers.

Contributions and organizational structure

In summary, this study makes the following key contributions:

- Proposing an improved multivariate grey prediction model. To maximize the information obtained from data, a more enhanced multivariate grey model called FBNGM (1, N, r) is introduced. This upgraded model incorporates the use of a whale optimization algorithm to optimize both the fractional operator and the background value coefficient. As a result, it is expected to enhance the impact of novel information and improve the accuracy of predictions.
- Adequate introduction of various influences to construct CO_2 emissions prediction models. Different from previous CO_2 emission prediction models, this study not only introduces economic, energy, industrial, and other factors, but also establishes three univariate, three multivariate models, and three non-grey multivariate prediction models to predict CO_2 emissions, and eventually confirms the inseparable relationship between CO_2 emissions and the various influencing factors, as well as the outstanding forecasting accuracy demonstrated by the proposed model.
- Performing two numerical cases, results analysis, and future forecasting. To assess the effectiveness and robustness of the proposed model, this study employs two numerical cases of CO_2 emissions per capita obtained from the World Bank and calculated based on energy consumption. This study not only compares the mean absolute error (MAE), absolute percentage error (APE), mean absolute percentage error (MAPE), and root mean square error (RMSE) of the nine models, but also predicts the CO_2 emissions per capita by 2030 according to the established FBNGM (1, N, r) model and finally puts forward relevant suggestions for relevant decision-makers to refer.

Other organizational structures of this study are as follows: "Literature research" provides a review of the relevant studies that have projected CO_2. "Methods" introduces and validates the FBNGM (1, N, r) model proposed by this study. Afterwards, "Model application" presents and discusses the numerical simulation results obtained from applying the FBNGM (1, N, r) model. Based on the forecasting results, "Discussion and policy suggestions" provides several recommendations. Finally, concluding remarks are given in "Conclusion."

Literature research

Many researchers have proposed a wide range of CO_2 emission forecasting models to enhance the accuracy of predictions. These models can be broadly classified into three categories: statistical models (Weng et al. 2020), artificial intelligence models (Weng et al. 2022; Delanoë et al. 2023), and grey prediction models. In order to further enhance the predictive capabilities of these models, researchers have incorporated relevant factors such as economic, social, and demographic variables.

Factors affecting carbon dioxide emissions

The selection of influencing factors is critical to accurately forecasting CO_2 emissions. It is important to rely on reliable data and scientific methods, consider causality and correlation, and ensure the observability and availability of factors (Jian et al. 2021).

CO_2 emissions are often influenced by economic, demographic, and social factors. Economic development plays a vital role in determining CO_2 emissions. Generally, as the economy develops, there is an increased demand for energy, particularly fossil fuels, which leads to a rise in CO_2 emissions (He et al. 2022). Continuous population growth has led to a corresponding increase in industrial production, transportation, and agricultural activities, further contributing to CO_2 emissions (Huo et al. 2023). Income levels also strongly correlate with CO_2 emissions, as higher-income countries and individuals are more capable of implementing measures that help reduce CO_2 emissions. Conversely, low-income levels often face greater economic pressures and development needs, posing challenges in reducing CO_2 emissions. Energy and industrial infrastructure also contribute significantly to CO_2 emissions. As sustainable energy sources such as solar and wind become more common, the energy mix will gradually shift toward low-carbon solutions (Mohsin et al. 2022). Similarly, the industrial structure is shifting from high-emission to low-emission sectors, resulting in lower CO_2 emissions (He et al. 2022). In addition, the pace of urbanization greatly impacts CO_2 emissions. As urban areas expand, the population in cities increases, leading to greater demand for infrastructure and transportation, subsequently driving up energy consumption and CO_2 emissions (Mohsin et al. 2019).

Statistical models

Statistical modeling is a well-known method to extrapolate future CO_2 emission trends based on historical data and relevant factors. This helps to understand the changing patterns of CO_2 emissions, assess the effectiveness of environmental policies, and formulate sustainable development strategies (Ding and Zhang 2023).

The linear regression model is a widely used statistical approach that relies on a linear equation. In this model, the dependent variable is CO_2 emissions, while the independent variables represent the associated factors. By analyzing historical data and fitting the model, researchers can assess the extent to which each independent variable affects CO_2 emissions. Moreover, this model facilitates the prediction of future emissions by leveraging these established relationships. Meng and Niu (2011) employed a logistic regression model to predict CO_2 emissions from various industries, such as industry, agriculture, and transportation. Xu et al. (2019) discussed the problem of the nonlinear auto regressive model with exogenous inputs (NARX). According to their predictions, China's CO_2 emissions are expected to peak in 2029, 2031, and 2035 under low growth, moderate benchmark growth, and high growth scenarios, respectively. Karakurt and Aydin (2023) used regression models to project fossil fuel-related CO_2 emissions for the BRICS and MINT countries alone, and the results show that emissions will increase significantly in the future for both groups of countries.

In addition to linear regression models, several other statistical models can be used to predict CO_2 emissions. For example, time series analysis models can capture seasonal, trend, and cyclical variations in emissions. These models can be adjusted for different data characteristics to improve the accuracy of the forecast. In a study conducted by Chen et al. (2022a), the STRPAT method was employed to identify factors influencing CO_2 emissions from energy consumption in 30 regions in China. They combined this approach with an ARIMA model to predict the trend of CO_2 emissions in 2023, revealing a continued increase in China's emissions and a widening disparity in CO_2 emissions per capita among provinces.

However, the statistical analysis model can produce accurate prediction results heavily depending on sufficient data input for parameter estimation (Wu et al. 2015). These models make inferences based on historical data and known factors, but they may not fully capture all the complexities and uncertainties of the future. Therefore, when using statistical models for CO_2 emission forecasting, it is imperative to exercise caution when interpreting the results and to complement them with insights from other disciplines and expert judgment.

Artificial intelligence models

The use of artificial intelligence (AI) models in predicting CO_2 emissions is becoming more common. As the amount of data increases and computational power improves, AI models can deal with complex nonlinear relationships to provide more accurate CO_2 emission predictions.

In real-world problems, single or hybrid AI models are usually used for prediction. Ren and Long (2021) predicted the carbon emissions of Guangdong Province from 2020 to 2060 using a fast-learning network (FLN) improved by the chicken swarm optimization (CSO) algorithm, verified the superiority of the model by three indicators, MAE, MAPE, and RMSE, and set up nine scenarios to explore the low-carbon development path. To ensure precise forecasting of Turkey's transportation-related CO_2 emissions, Ağbulut (2022) employed three artificial intelligence techniques for prediction. There is also an interaction between the price fluctuation of fossil energy and CO_2 emissions. Kassouri et al. (2022) analyzed the coordinated movement between the US oil shock and the intensity of CO_2 emissions through a wavelet model. The study found that the rise in oil prices caused by the impact of oil demand and global economic activities cannot replace environmental policies aimed at reducing carbon emissions. Kong et al. (2022) assembled ensemble empirical mode decomposition (EEMD) and variational mode decomposition (VMD) to decompose the original data twice, applied partial autocorrelation function to select the optimal model inputs, and finally predicted the carbon emissions by long and short-term memory (LSTM) neural networks. The results show that the quadratic decomposition technique can improve the accuracy of the model, and the proposed model exhibits excellent accuracy compared with 12 other models.

It is important to note that AI models still face some challenges in predicting CO_2 emissions. The quality and quantity of data are critical for AI models to predict CO_2 emissions, and large-scale, high-quality datasets can provide more accurate model training and prediction results. As a result, incomplete data, uncertainty, and non-linear relationships may affect the accuracy of the models.

Grey prediction models

Artificial intelligence methods typically focus on big data and large samples, requiring a large amount of historical data, and statistical models rely on data for parameter estimation. However, predicting CO_2 emissions is a complex and dynamic issue influenced by various factors, including economic and social aspects. As society continues to evolve, it becomes increasingly important to consider the impact of new information. In situations characterized by limited or incomplete information, the grey prediction model has

emerged as a valuable and effective technique (Liu et al. 2012). In recent decades, numerous researchers have introduced a range of extensible and innovative models built upon the foundation of the GM (1, 1) model, which serves as the fundamental grey model (Liu and Deng 2000). The GM (1, 1) model has undergone advancements and enhancements, which can be observed primarily in three aspects: optimization of model parameters (Yu et al. 2021), expansion of model structure (Zeng and Li 2021), and construction of combined models (Chen et al. 2021).

For the univariate grey prediction model, Wu et al. (2020) used a conformable fractional non-homogeneous grey model (CFNGM (1, 1, k, c)) to study the CO_2 emissions of the BRICS countries and predicted the emissions from 2019 to 2025 based on the model. The results demonstrated that the CFNGM (1, 1, k, c) model outperformed other models in prediction accuracy. Xie et al. (2021) introduced a continuous consistent fractional nonlinear grey Bernoulli model (CCFNGBM (1, 1)) for predicting CO_2 emissions resulting from fuel combustion in China. The parameters of the model are optimized by the Grey Wolf optimization (GWO) algorithm, and the experimental results showed that the prediction accuracy of the newly proposed optimized model was better than that of other benchmark models. Gao et al. (2022) created a fractional cumulative grey Gompertz model (FAGGM (1, 1)) based on Gompertz differential equations, which was validated on six carbon emission datasets, and the proposed model achieved the best predictions in all cases.

To conduct a comprehensive analysis of the factors that impact carbon emissions, building on the traditional multivariable model GM (1, N) (Tien 2012), Zeng et al. (2016) incorporated a linear correction term and the grey action quantity to enhance its structure, culminating in the development of the NGM (1, N) model. Experimental results verify that the model with improved structure yields higher prediction accuracy. Ding et al. (2020) identified the relevant influencing factors and established their strong nonlinear effects through grey relational analysis. Subsequently, they devised the discrete grey power model (DGPM (1, N)), capable of accounting for these nonlinear factors. Ye et al. (2021) introduced a new multivariate grey model with time delay, known as ATGM (1, N), for assessing the cumulative effects of CO_2 emissions in China's transportation industry. Findings demonstrated that the model surpasses six competing models, which included DGM (1, N), GMC (1, N), DDGM (1, N), CDGM (1, N), MDL, and SVR. Wan et al. (2022) developed a grey multivariate prediction model based on dummy variables and their interactions for predicting CO_2 emissions from primary energy consumption in Guangdong Province, and the prediction accuracies of the new model were 2.87% and 0.86% in the simulation and prediction phases, respectively, which were significantly better than those of the other three competing models. Ding et al. (2023b) developed a new grey multivariate coupled model (CTGM (1, N)) for carbon emission prediction to fit the CO_2 emissions of three countries, namely, China, the USA, and Japan, which introduced Choquet fuzzy integrals and grey multivariate delays and was compared with six reference models. The results of the performance tests demonstrated that the CTGM (1, N) model exhibits remarkable stability in predicting carbon emissions.

The grey prediction model described above has shown promising results in predicting CO_2 emissions. However, to further enhance the accuracy of the predictions, it is suggested to incorporate fractional-order cumulative operators and optimized background value coefficients. By introducing these elements, the model has the potential to enhance the precision of its predictions. Furthermore, by optimizing the relevant parameters through the use of optimization algorithms, the effectiveness of the model can be greatly improved.

Although much academic attention has been devoted to CO_2 emissions, previous studies on CO_2 emission projections have primarily focused on specific countries or regions, rather than considering per capita emissions, and have led to differences in projection results due to different data and influencing factors. And it is still a difficult research problem to synthesize the various factors and obtain accurate predictions. Therefore, this study proposes a novel multivariate grey prediction model, which optimizes fractional order and background value coefficients to predict CO_2 emissions per capita. The model considers the contribution of human activities to CO_2 emissions, acknowledging the significant role of humans in driving carbon emissions. Moreover, the study incorporates various factors that impact carbon emissions into the prediction model, aiming to enhance its accuracy and reliability.

Methods

This section primarily introduces the proposed FBNGM (1, N, r) model and its related properties, along with the utilization of the whale optimization algorithm (WOA) (Mirjalili and Lewis 2016). Building on the NGM (1, N) model, initially introduced by Zeng et al. (2016), this study incorporates fractional order operators, background value coefficient, and the WOA algorithm to enhance the predictive accuracy of the NGM (1, N) model. In particular, through the utilization of the WOA algorithm, the fractional operator and background value of the FBNGM (1, N, r) model are optimized with effectiveness.

FBNGM (1, N, r) model

Definition 1. Assume $\boldsymbol{Y}^{(0)} = \left(y^{(0)}(1), y^{(0)}(2), \cdots, y^{(0)}(n)\right)$ is a characteristic variable sequence, $\boldsymbol{X}_k^{(0)} = \left(x_k^{(0)}(1), x_k^{(0)}(2), \cdots, x_k^{(0)}(n)\right), k = 2, 3, \cdots N$ is the sequence of driving variable. $\boldsymbol{Y}^{(1)} = \left(\boldsymbol{y}^{(1)}(1), \boldsymbol{y}^{(1)}(2), \cdots, \boldsymbol{y}^{(1)}(n)\right)$ and $\boldsymbol{X}_k^{(1)} = \left(\boldsymbol{x}_k^{(1)}(1), \boldsymbol{x}_k^{(1)}(2), \cdots, \boldsymbol{x}_k^{(1)}(n)\right), k = 2, 3, \cdots, N$ are called first-order accumulated generating operation (1-AGO) sequences of $\boldsymbol{Y}^{(0)}$ and $\boldsymbol{X}_k^{(0)}$, respectively.where

$$\boldsymbol{y}^{(1)}(i) = \sum_{t=1}^{i} y^{(0)}(t), i = 1, 2, \cdots, n \tag{1}$$

$$\boldsymbol{x}_k^{(1)}(i) = \sum_{t=1}^{i} x_k^{(0)}(t), i = 1, 2, \cdots, n \tag{2}$$

Definition 2. Assume $\boldsymbol{Y}^{(0)}$ and $\boldsymbol{X}_k^{(0)}$ are the initial sequence, $\boldsymbol{Y}^{(r)} = \left(\boldsymbol{y}^{(r)}(1), \boldsymbol{y}^{(r)}(2), \cdots \boldsymbol{y}^{(r)}(n)\right)$ and $\boldsymbol{X}_k^{(r)} = \left(\boldsymbol{x}_k^{(r)}(1), \boldsymbol{x}_k^{(r)}(2), \cdots, \boldsymbol{x}_k^{(r)}(n)\right)$ are called r-order accumulating generation (r-AGO) sequences of $\boldsymbol{Y}^{(0)}$ and $\boldsymbol{X}_k^{(0)}$, respectively.where

$$\boldsymbol{y}^{(r)}(i) = \sum_{t=1}^{i} \frac{\boldsymbol{\Gamma}(r+i-t)}{\boldsymbol{\Gamma}(i-t+1)\boldsymbol{\Gamma}(r)} y^{(0)}(t), i = 1, 2, \cdots, n \tag{3}$$

$$\boldsymbol{x}_k^{(r)}(i) = \sum_{t=1}^{i} \frac{\boldsymbol{\Gamma}\left(r_k+i-t\right)}{\boldsymbol{\Gamma}(i-t+1)\boldsymbol{\Gamma}\left(r_k\right)} x_k^{(0)}(t), i = 1, 2, \cdots, n \tag{4}$$

$\boldsymbol{Y}^{(r-1)} = \left(\boldsymbol{y}^{(r-1)}(1), \boldsymbol{y}^{(r-1)}(2), \cdots \boldsymbol{y}^{(r-1)}(n)\right)$ is a sequence of $(r-1)$-order accumulating generation ($(r-1)$-AGO) sequences obtained through a transformation of the sequence $\boldsymbol{Y}^{(0)}$.where

$$\boldsymbol{y}^{(r-1)}(i) = \sum_{t=1}^{i} \frac{\boldsymbol{\Gamma}(r-1+i-t)}{\boldsymbol{\Gamma}(i-t+1)\boldsymbol{\Gamma}(r-1)} y^{(0)}(t), i = 1, 2, \cdots, n \tag{5}$$

$\boldsymbol{Z}^{(r)} = \left(z^{(r)}(1), z^{(r)}(2), \cdots, z^{(r)}(n)\right)$ is a background value sequence generated by the neighboring elements of $\boldsymbol{Y}^{(r)}$,where

$$z^{(r)}(i) = \xi \times \boldsymbol{y}^{(r)}(i) + (1-\xi) \times \boldsymbol{y}^{(r)}(i-1), \xi \in (0, 1), i = 2, 3, \cdots, n \tag{6}$$

Theorem 1. Suppose $\boldsymbol{Y}^{(r)}$, $\boldsymbol{X}_k^{(r)}$, and $\boldsymbol{Z}^{(r)}$ are defined as **Definitions 1** and **2**, the FBNGM (1, N, r) model, which is a fractional multivariable grey prediction model with background value optimization, can be mathematically represented as follows:

$$\boldsymbol{y}^{(r-1)}(i) + pz^{(r)}(i) = \sum_{k=2}^{N} m_k \boldsymbol{x}_k^{(r)}(i) + q_1(i-1) + q_2, i = 1, 2, \cdots, n \tag{7}$$

where p is the system development coefficient, $m_k x_k^{(r)}(i)$ is the driving term, and $q_1(i-1)$ and q_2 are the linear correction term and the grey action quantity term, respectively.

Definition 3. Assume $\boldsymbol{Y}^{(0)}$ is the initial sequence, $\boldsymbol{Y}^{(-r)} = \left(\boldsymbol{y}^{(-r)}(1), \boldsymbol{y}^{(-r)}(2), \cdots \boldsymbol{y}^{(-r)}(n)\right)$ is the r-order inverse accumulating generation (r-IAGO) sequence of $\boldsymbol{Y}^{(0)}$,where

$$\boldsymbol{y}^{(-r)}(i) = \sum_{t=0}^{i-1} (-1)^t \frac{\boldsymbol{\Gamma}(r+1)}{\boldsymbol{\Gamma}(t+1)\boldsymbol{\Gamma}(r-t+1)} y^{(0)}(i-t), i = 1, 2, \cdots, n \tag{8}$$

Theorem 2. Let $\boldsymbol{Y}^{(r-1)} = \left(\boldsymbol{y}^{(r-1)}(1), \boldsymbol{y}^{(r-1)}(2), \cdots, \boldsymbol{y}^{(r-1)}(n)\right)$ be the $(r-1)$-order accumulating generation sequence of $Y^{(0)}$. Assume that $\boldsymbol{Y}^{(0)}$, $\boldsymbol{X}_k^{(r)}$, and $\boldsymbol{Z}^{(r)}$ have been defined in **Definitions 1** and **2**. Then, the estimated parameter vector, i.e., $\widehat{\boldsymbol{g}} = \left[m_2, m_3, \cdots, m_N, p, q_1, q_2\right]^T$, of FBNGM (1, N, r) satisfies:

(i) if $n = N + 3$ and $|\boldsymbol{M}| \neq 0$ then $\widehat{\boldsymbol{g}} = \boldsymbol{M}^{-1}\boldsymbol{W}$;
(ii) if $n > N + 3$ and $\left|\boldsymbol{M}^T\boldsymbol{M}\right| \neq 0$ then $\widehat{\boldsymbol{g}} = \left(\boldsymbol{M}^T\boldsymbol{M}\right)^{-1}\boldsymbol{M}^T\boldsymbol{W}$;
(iii) if $n < N + 3$ and $\left|\boldsymbol{M}\boldsymbol{M}^T\right| \neq 0$ then $\widehat{\boldsymbol{g}} = \boldsymbol{M}^T\left(\boldsymbol{M}\boldsymbol{M}^T\right)^{-1}\boldsymbol{W}$

where

$$\boldsymbol{M} = \begin{pmatrix} \boldsymbol{x}_2^{(r)}(2) & \boldsymbol{x}_3^{(r)}(2) & \cdots & \boldsymbol{x}_N^{(r)}(2) & -z^{(r)}(2) & 1 & 1 \\ \boldsymbol{x}_2^{(r)}(3) & \boldsymbol{x}_3^{(r)}(3) & \cdots & \boldsymbol{x}_N^{(r)}(3) & -z^{(r)}(3) & 2 & 1 \\ \vdots & \vdots & & \vdots & \vdots & \vdots & \vdots \\ \boldsymbol{x}_2^{(r)}(n) & \boldsymbol{x}_3^{(r)}(n) & \cdots & \boldsymbol{x}_N^{(r)}(n) & -z^{(r)}(n) & n-1 & 1 \end{pmatrix}, \boldsymbol{W} = \begin{pmatrix} \boldsymbol{y}^{(r-1)}(2) \\ \boldsymbol{y}^{(r-1)}(3) \\ \vdots \\ \boldsymbol{y}^{(r-1)}(n) \end{pmatrix}$$

Proof. Substitute $i = 2, 3, \cdots n$ into Eq. (7), we can obtain

$$\begin{cases} \boldsymbol{y}^{(r-1)}(2) = \sum_{k=2}^{N} m_k \boldsymbol{x}_k^{(r)}(2) - pz^{(r)}(2) + q_1 + q_2 \\ \boldsymbol{y}^{(r-1)}(3) = \sum_{k=2}^{N} m_k \boldsymbol{x}_k^{(r)}(3) - pz^{(r)}(3) + 2q_1 + q_2 \\ \vdots \\ \boldsymbol{y}^{(r-1)}(n) = \sum_{k=2}^{N} m_k \boldsymbol{x}_k^{(r)}(n) - pz^{(r)}(n) + (n-1)q_1 + q_2 \end{cases} \tag{9}$$

The matrix form of Eq. (9) is

$$\boldsymbol{W} = \boldsymbol{M}\widehat{\boldsymbol{g}} \tag{10}$$

(i) When $n = N + 3$ and $|\boldsymbol{M}| \neq 0$, then $\boldsymbol{M}$ is an invertible matrix; Eq. (10) has a unique solution.
(ii) When $n > N + 3$, $\boldsymbol{M}$ is a column full rank matrix and $\left|\boldsymbol{M}^T\boldsymbol{M}\right| \neq 0$, then $\boldsymbol{M}$ can be discomposed into the product of a $(n-1) \times (N+2)$ matrix $\boldsymbol{B}$ and a $(N+2) \times (N+2)$ matrix $\boldsymbol{C}$, i.e., $\boldsymbol{M} = \boldsymbol{B}\boldsymbol{C}$. Therefore, the generalized inverse matrix $\boldsymbol{M}^{\dagger}$ of $\boldsymbol{M}$ can be given by

$$\boldsymbol{M}^{\dagger} = \boldsymbol{C}^{T}\left(\boldsymbol{C}\boldsymbol{C}^{T}\right)^{-1}\left(\boldsymbol{B}^{T}\boldsymbol{B}\right)^{-1}\boldsymbol{B}^{T} \tag{11}$$

Then, the estimated parameter vector: $\widehat{\boldsymbol{g}}$ can be expressed as follows:

$$\widehat{\boldsymbol{g}} = \boldsymbol{C}^{T}\left(\boldsymbol{C}\boldsymbol{C}^{T}\right)^{-1}\left(\boldsymbol{B}^{T}\boldsymbol{B}\right)^{-1}\boldsymbol{B}^{T}\boldsymbol{W} \tag{12}$$

Since $\boldsymbol{M}$ is a column full-rank matrix, let $\boldsymbol{C} = \boldsymbol{I}_{N+2}$, we have

$$\boldsymbol{M} = \boldsymbol{B}\boldsymbol{C} = \boldsymbol{B}\boldsymbol{I}_{N+2} = \boldsymbol{B} \tag{13}$$

then

$$\begin{aligned}\widehat{\boldsymbol{g}} &= \boldsymbol{C}^{T}\left(\boldsymbol{C}\boldsymbol{C}^{T}\right)^{-1}\left(\boldsymbol{B}^{T}\boldsymbol{B}\right)^{-1}\boldsymbol{B}^{T}W \\ &= \boldsymbol{I}_{N+2}^{T}\left(\boldsymbol{I}_{N+2}\boldsymbol{I}_{N+2}^{T}\right)^{-1}\left(\boldsymbol{M}^{T}\boldsymbol{M}\right)^{-1}\boldsymbol{M}^{T}W = \left(\boldsymbol{M}^{T}\boldsymbol{M}\right)^{-1}\boldsymbol{M}^{T}W\end{aligned} \tag{14}$$

(iii) When $n < N+3$, $\boldsymbol{M}$ is a row full-rank matrix and $\left|\boldsymbol{M}^{T}\boldsymbol{M}\right| \neq 0$, then $\boldsymbol{M}$ can be discomposed into

$$\boldsymbol{M} = \boldsymbol{I}_{m-1}\boldsymbol{C} \tag{15}$$

Similar to point (ii), we can rewrite Eq. (12) as

$$\begin{aligned}\widehat{\boldsymbol{g}} &= \boldsymbol{C}^{T}\left(\boldsymbol{C}\boldsymbol{C}^{T}\right)^{-1}\left(\boldsymbol{B}^{T}\boldsymbol{B}\right)^{-1}\boldsymbol{B}^{T}W \\ &= \boldsymbol{M}^{T}\left(\boldsymbol{M}\boldsymbol{M}^{T}\right)^{-1}\left(\boldsymbol{I}_{m-1}^{T}\boldsymbol{I}_{m-1}\right)^{-1}\boldsymbol{I}_{m-1}^{T}W = \boldsymbol{M}^{T}\left(\boldsymbol{M}^{T}\boldsymbol{M}\right)^{-1}W\end{aligned} \tag{16}$$

End of proof.

Theorem 3. Given $\boldsymbol{M}$, $\boldsymbol{W}$, and $\widehat{\boldsymbol{g}}$ as stated in **Theorem 2**, then.

(i) Expressed below is the time-response equation for the model in Eq. (7)

$$\begin{aligned}\widehat{\boldsymbol{y}}^{(r)}(i) = &\sum_{u=1}^{i-1}\left[\boldsymbol{\eta}_1\sum_{k=2}^{N}\boldsymbol{\eta}_2^{u-1}\boldsymbol{m}_k\boldsymbol{x}_k^{(r)}(i-u+1)\right] \\ &+\boldsymbol{\eta}_2^{i-1}\widehat{\boldsymbol{y}}^{(r)}(1) + \sum_{j=0}^{i-2}\boldsymbol{\eta}_2^{j}\left[(i-j)\boldsymbol{\eta}_3 + \boldsymbol{\eta}_4\right]\end{aligned} \quad i = 1, 2, \cdots, n, \tag{17}$$

(ii) Below is the final restored form of the FBNGM (1, N, r) model:

$$\begin{aligned}\widehat{\boldsymbol{y}}^{(0)}(i) = &\sum_{t=0}^{i-1}(-1)^{t}\frac{\boldsymbol{\Gamma}(r+1)}{\boldsymbol{\Gamma}(t+1)\boldsymbol{\Gamma}(r-t+1)} \\ &\left\{\sum_{u=1}^{i-1}\left[\boldsymbol{\eta}_1\sum_{k=2}^{N}\boldsymbol{\eta}_2^{u-1}\boldsymbol{m}_k\boldsymbol{x}_k^{(r)}(i-u+1)\right]\right. \quad i = 1, 2, \cdots, n \\ &\left.+\boldsymbol{\eta}_2^{i-1}\widehat{\boldsymbol{y}}^{(r)}(1) + \sum_{j=0}^{i-2}\boldsymbol{\eta}_2^{j}\left[(i-j)\boldsymbol{\eta}_3 + \boldsymbol{\eta}_4\right]\right\}\end{aligned} \tag{18}$$

where

$\widehat{\boldsymbol{y}}^{(r)}(1) = y^{(0)}(1)$, $\eta_1 = \frac{1}{1+p\xi}$, $\eta_2 = \frac{1-p+p\xi}{1+p\xi}$, $\eta_3 = \frac{q_1}{1+p\xi}$, $\eta_4 = \frac{q_2}{1+p\xi}$

The proof of (i). According to **Definition 2** and **Theorem 1**, we have

$$\boldsymbol{y}^{(r-1)}(i) = \sum_{k=2}^{N}\boldsymbol{m}_k\boldsymbol{x}_k^{(r)}(i) - pz^{(r)}(i) + q_1(i-1) + q_2 \tag{19}$$

$$z^{(r)}(i) = \xi\times\boldsymbol{y}^{(r)}(i) + (1-\xi)\times\boldsymbol{y}^{(r)}(i-1) \tag{20}$$

Since

$$\boldsymbol{y}^{(r-1)}(i) = \boldsymbol{y}^{(r)}(i) - \boldsymbol{y}^{(r)}(i-1) \tag{21}$$

Substituting Eqs. (21) and (20) into Eq. (19), we have

$$\begin{aligned}\widehat{\boldsymbol{y}}^{(r)}(i) - \widehat{\boldsymbol{y}}^{(r)}(i-1) = &\sum_{k=2}^{N}\boldsymbol{m}_k\boldsymbol{x}_k^{(r)}(i) \\ &- p\left[\xi\times\widehat{\boldsymbol{y}}^{(r)}(i) + (1-\xi)\times\widehat{\boldsymbol{y}}^{(r)}(i-1)\right] \\ &+ q_1(i-1) + q_2\end{aligned} \tag{22}$$

Then, we can obtain

$$\begin{aligned}\widehat{\boldsymbol{y}}^{(r)}(i) = &\frac{1}{1+p\xi}\sum_{k=2}^{N}\boldsymbol{m}_k\boldsymbol{x}_k^{(r)}(i) + \frac{1-p+p\xi}{1+p\xi}\widehat{\boldsymbol{y}}(i-1) \\ &+ \frac{q_1}{1+p\xi}(i-1) + \frac{q_2-q_1}{1+p\xi}\end{aligned} \tag{23}$$

Let

$\eta_1 = \frac{1}{1+p\xi}, \eta_2 = \frac{1-p+p\xi}{1+p\xi}, \eta_3 = \frac{q_1}{1+p\xi}, \eta_4 = \frac{q_2-q_1}{1+p\xi}$

Then, Eq. (23) becomes

$$\widehat{\boldsymbol{y}}^{(r)}(i) = \eta_1\sum_{k=2}^{N}\boldsymbol{m}_k\boldsymbol{x}_k^{(r)}(i) + \eta_2\widehat{\boldsymbol{y}}(i-1) + \eta_3 i + \eta_4 \tag{24}$$

According to Eq. (24), when $i=2$, we get

$$\widehat{\boldsymbol{y}}^{(r)}(2) = \eta_1\sum_{k=2}^{N}m_k\boldsymbol{x}_k^{(r)}(2) + \eta_2\widehat{\boldsymbol{y}}(1) + 2\eta_3 + \eta_4 \tag{25}$$

When $i=3$, we have

$$\widehat{\boldsymbol{y}}^{(r)}(3) = \eta_1\sum_{k=2}^{N}m_k\boldsymbol{x}_k^{(r)}(3) + \eta_2\widehat{\boldsymbol{y}}(2) + 3\eta_3 + \eta_4 \tag{26}$$

Substituting Eq. (25) into Eq. (26), we obtain

$$\begin{aligned}\hat{\boldsymbol{y}}^{(r)}(3) &= \eta_1 \sum_{k=2}^{N} m_k \boldsymbol{x}_k^{(r)}(3) + \eta_2 \left[\eta_1 \sum_{k=2}^{N} m_k \boldsymbol{x}_k^{(r)}(2) + \eta_2 \hat{\boldsymbol{y}}(1) + 2\eta_3 + \eta_4 \right] \\ &\quad + 3\eta_3 + \eta_4 \\ &= \eta_1 \sum_{k=2}^{N} m_k \boldsymbol{x}_k^{(r)}(3) + \eta_2 \eta_1 \sum_{k=2}^{N} m_k \boldsymbol{x}_k^{(r)}(2) \\ &\quad + \eta_2^2 \hat{\boldsymbol{y}}(1) + 2\eta_2 \eta_3 + \eta_2 \eta_4 + 3\eta_3 + \eta_4 \end{aligned} \tag{27}$$

No general expression can be found from Eq. (27), so we need to continue to so the derivation.

When $i = 4$, we can get

$$\hat{\boldsymbol{y}}^{(r)}(4) = \eta_1 \sum_{k=2}^{N} m_k \boldsymbol{x}_k^{(r)}(4) + \eta_2 \hat{\boldsymbol{y}}(3) + 4\eta_3 + \eta_4 \tag{28}$$

By substituting Eq. (27) into Eq. (28), we can derive

$$\begin{aligned}\hat{\boldsymbol{y}}^{(r)}(4) &= \eta_1 \sum_{k=2}^{N} m_k \boldsymbol{x}_k^{(r)}(4) + \eta_1 \eta_2 \sum_{k=2}^{N} m_k \boldsymbol{x}_k^{(r)}(3) + \eta_1 \eta_2^2 \sum_{k=2}^{N} m_k \boldsymbol{x}_k^{(r)}(2) \\ &\quad + \eta_2^3 \hat{\boldsymbol{y}}(1) + 2\eta_2^2 \eta_3 + \eta_2^2 \eta_4 + 3\eta_2 \eta_3 + \eta_2 \eta_4 + 4\eta_3 + \eta_4 \end{aligned} \tag{29}$$

$$\vdots$$

When $i = v$, we can get

$$\begin{aligned}\hat{\boldsymbol{y}}^{(r)}(v) =& \eta_1 \sum_{k=2}^{N} m_k \boldsymbol{x}_k^{(r)}(v) + \eta_1 \eta_2 \sum_{k=2}^{N} m_k \boldsymbol{x}_k^{(r)}(v-1) \\ &+ \cdots + \eta_1 \eta_2^{v-2} \sum_{k=2}^{N} m_k \boldsymbol{x}_k^{(r)}(2) + \eta_2^{v-1} \hat{\boldsymbol{y}}(1) \\ &+ 2\eta_2^{v-2} \eta_3 + \eta_2^{v-2} \eta_4 + 3\eta_2^{v-3} \eta_3 + \eta_2^{v-3} \eta_4 + \cdots + v\eta_3 + \eta_4 \end{aligned} \tag{30}$$

In Eq. (30), let

$$\begin{aligned} E &= \eta_1 \sum_{k=2}^{N} m_k \boldsymbol{x}_k^{(r)}(v) + \eta_1 \eta_2 \sum_{k=2}^{N} m_k \boldsymbol{x}_k^{(r)}(v-1) \\ &\quad + \cdots + \eta_1 \eta_2^{v-2} \sum_{k=2}^{N} m_k \boldsymbol{x}_k^{(r)}(2) \\ &= \sum_{u=1}^{v-1} \left[\eta_1 \sum_{k=2}^{N} \eta_2^{u-2} m_k \boldsymbol{x}_k^{(r)}(v-u+1) \right] \end{aligned}$$

$$\begin{aligned} F &= 2\eta_2^{v-2} \eta_3 + \eta_2^{v-2} \eta_4 + 3\eta_2^{v-3} \eta_3 + \eta_2^{v-3} \eta_4 + \cdots + v\eta_3 + \eta_4 \\ &= \textstyle\sum_{j=0}^{v-2} \eta_2^j \left[(v-j)\eta_3 + \eta_4 \right] \end{aligned}$$

By substituting $\boldsymbol{E}$ and $\boldsymbol{F}$ into Eq. (30), then Eq. (30) can be simplified as

$$\begin{aligned}\hat{\boldsymbol{y}}^{(r)}(i) =& \textstyle\sum_{u=1}^{i-1} \left[\eta_1 \sum_{k=2}^{N} \eta_2^{u-1} m_k \boldsymbol{x}_k^{(r)}(i-u+1) \right] \\ &+ \eta_2^{i-1} \hat{\boldsymbol{y}}^{(r)}(1) + \textstyle\sum_{j=0}^{i-2} \eta_2^j \left[(i-j)\eta_3 + \eta_4 \right] \end{aligned} \tag{31}$$

The proof of (ii). According to the **Definition 3**

$$\boldsymbol{y}^{(-r)}(i) = \sum_{t=0}^{i-1} (-1)^t \frac{\boldsymbol{\Gamma}(r+1)}{\boldsymbol{\Gamma}(t+1)\boldsymbol{\Gamma}(r-t+1)} y^{(0)}(i-t), i = 1, 2, \cdots, n$$

Then, we have

$$\hat{\boldsymbol{y}}^{(0)}(i) = \sum_{t=0}^{i-1} (-1)^t \frac{\boldsymbol{\Gamma}(r+1)}{\boldsymbol{\Gamma}(t+1)\boldsymbol{\Gamma}(r-t+1)} \hat{\boldsymbol{y}}^{(r)}(i), i = 1, 2, \cdots, n \tag{32}$$

By substituting Eq. (31) into Eq. (32), we can obtain the ultimate prediction equation for the FBNGM (1, N, r) model, which is presented below:

$$\begin{aligned}\hat{\boldsymbol{y}}^{(0)}(i) =& \sum_{t=0}^{i-1} (-1)^t \frac{\boldsymbol{\Gamma}(r+1)}{\boldsymbol{\Gamma}(t+1)\boldsymbol{\Gamma}(r-t+1)} \\ &\left\{ \sum_{u=1}^{i-1} \left[\eta_1 \sum_{k=2}^{N} \eta_2^{u-1} m_k \boldsymbol{x}_k^{(r)}(i-u+1) \right] \right. \\ &\left. + \eta_2^{i-1} \hat{\boldsymbol{y}}^{(r)}(1) + \sum_{j=0}^{i-2} \eta_2^j \left[(i-j)\eta_3 + \eta_4 \right] \right\} \end{aligned} \tag{33}$$

where $i = 1, 2, \cdots, n$.

End of proof.

Therefore, Eq. (33) can be used to calculate the simulated and predicted values.

Whale optimization algorithm

Basic idea

The whale optimization algorithm (WOA) was introduced by Mirjalili and Lewis (2016), inspired by the hunting tactics of whales in their natural environment. The main goal of developing the WOA algorithm was to replicate the effective hunting strategies used by whales to solve complex optimization problems more efficiently. When a group of whales hunts together, one whale will inevitably find the prey first. When this happens, other whales will swim towards the successful whale to compete for the prey.

The WOA algorithm stands out due to its ability to mimic the hunting behavior of humpback whales, achieved by combining both optimal and random individuals. It also emulates the spiral movement patterns observed in humpback whales during bubble net attacks. The three phases of whales' predatory behavior, which include encircling prey, bubble-net attacking, and active search for food, are all integrated into the WOA algorithm.

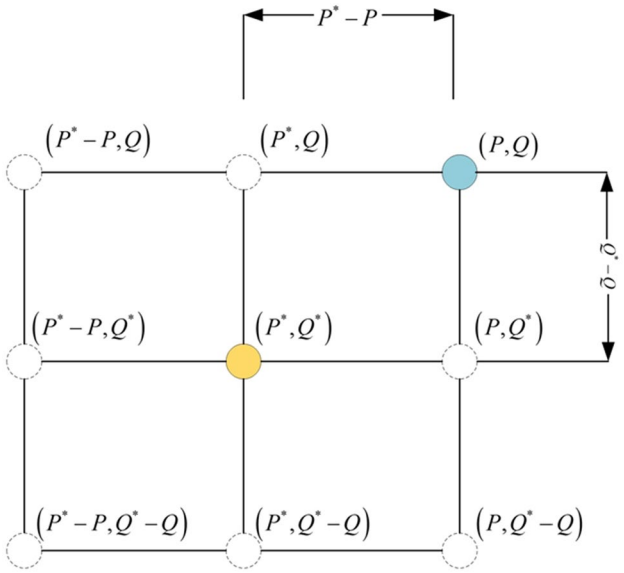

Fig. 2 Position vector and possible next location of the whale (Mirjalili and Lewis 2016)

Mathematical model

This section delineates how the WOA algorithm models the three distinct predatory behaviors utilized by humpback whales: encircling prey, bubble-net attacking, and actively searching for prey, all expressed mathematically.

Encircling prey Consider an optimization problem in a d-dimensional space, which has the position vector $\vec{\boldsymbol{P}}^*(t)$ of the optimal whale individual and the position vector $\vec{\boldsymbol{P}}(t)$ of a whale individual at iteration t. At the $(t+1)$-th iteration, the position vector of a whale individual, denoted as $\vec{\boldsymbol{P}}(t+1)$, is affected by the presence of an optimal whale individual. The iterative formulas are as follows:

$$\vec{\boldsymbol{P}}(t+1) = \vec{\boldsymbol{P}}^*(t) - \vec{\boldsymbol{M}} \cdot \vec{\boldsymbol{N}} \tag{34}$$

$$\vec{\boldsymbol{N}} = |\vec{\boldsymbol{R}} \cdot \vec{\boldsymbol{P}}^*(t) - \vec{\boldsymbol{P}}(t)| \tag{35}$$

$$\vec{\boldsymbol{M}} = 2\vec{\boldsymbol{c}} \cdot \vec{\boldsymbol{s}}_1 - \vec{\boldsymbol{c}} \tag{36}$$

$$\vec{\boldsymbol{R}} = 2 \cdot \vec{\boldsymbol{s}}_2 \tag{37}$$

where || and · in the calculation formula of $\vec{\boldsymbol{N}}$ represent the absolute value and element by element multiplication, respectively. As the iteration progresses, the vector $\vec{\boldsymbol{c}}$ decreases steadily from an initial value of 2 to a final value of 0, following a linear pattern. $\vec{\boldsymbol{s}}_1$ and $\vec{\boldsymbol{s}}_2$ are random vectors in[0,1].

Figure 2 illustrates the principle of Eq. (35) for the 2D problem. By adjusting the values of $\vec{\boldsymbol{M}}$ and $\vec{\boldsymbol{R}}$, you can get the best position around the agent. Furthermore, the position of a search agent can be ascertained by making a comparison with the location of the optimal agent.

Bubble-net attacking One of the distinctive hunting techniques employed by humpback whales is bubble-net attacking. To mimic this behavior, two mathematical equations have been developed:

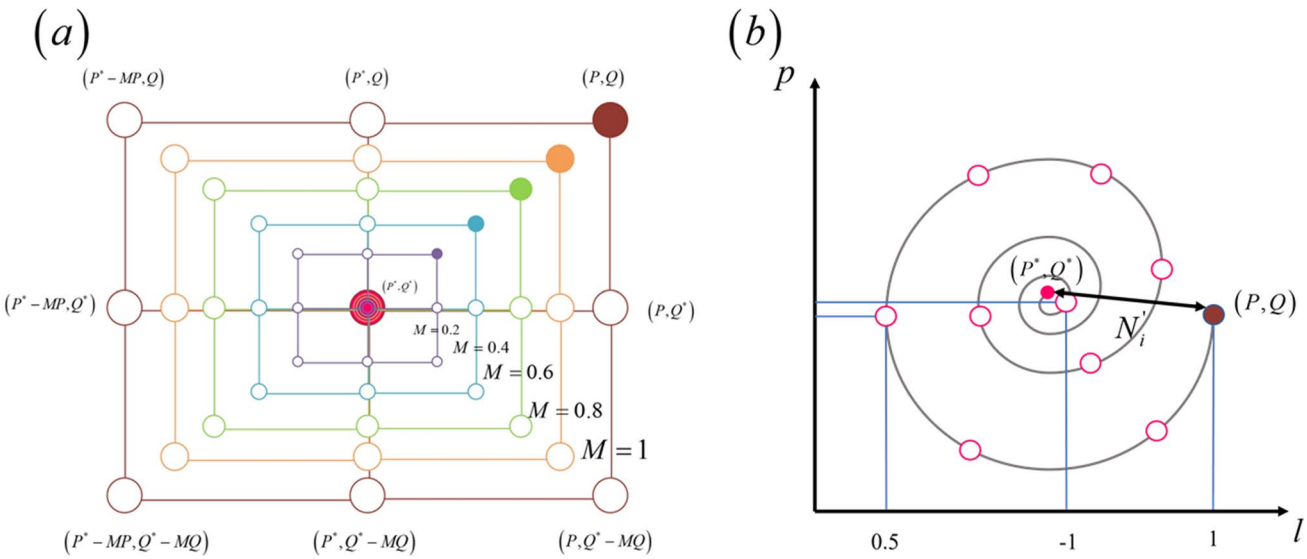

Fig. 3 Bubble-net search mechanism implemented in WOA: (**a**) shrinking encircling mechanism and (**b**) spiral updating position (Mirjalili and Lewis 2016)

a) Shrinking encircling mechanism

The mathematical model for the bubble-net attacking behavior closely resembles the previous model used to simulate the behavior of prey, with the primary difference being the range of values for $\overrightarrow{M}$ used in the equations. This behavior is achieved by decreasing $\vec{c}$ in Eq. (36). From Eq. (36), it can be seen that $\overrightarrow{M}$ will also decrease when $\vec{c}$ decreases. During each iteration, the vector $\overrightarrow{M}$ is a random value between $-c$ and c, where $\vec{c}$ linearly decreases from 2 to 0. That is, the range of $\overrightarrow{M}$ is $[-2, 2]$. Assuming that $\overrightarrow{M}$ is a random vector within the range of $[-1, 1]$, any point lying between the initial position and optimal position will serve as the new position for the whale. When $0 \le M \le 1$, all potential locations in 2D space that can be obtained by moving from point $(\boldsymbol{P}, \boldsymbol{Q})$ to point $(\boldsymbol{P}^*, \boldsymbol{Q}^*)$ are considered.

b) Spiral updating position

The process of this mechanism can be represented as shown in Fig. 3(b). In this way, the distance between the whale located at $(\boldsymbol{P}, \boldsymbol{Q})$ and prey located at $(\boldsymbol{P}^*, \boldsymbol{Q}^*)$ can be calculated. The spiral position update equation is as follows:

$$\overrightarrow{X}(t+1) = \overrightarrow{N}' \cdot e^{bl} \cdot \cos(2\pi l) + \vec{P}^*(t) \tag{38}$$

In the above equation, $\overrightarrow{N}' = \left|\vec{P}^*(t) - \vec{P}(t)\right|$ represents the distance between the whale and prey, b is a constant, l is a random number in $[-1, 1]$.

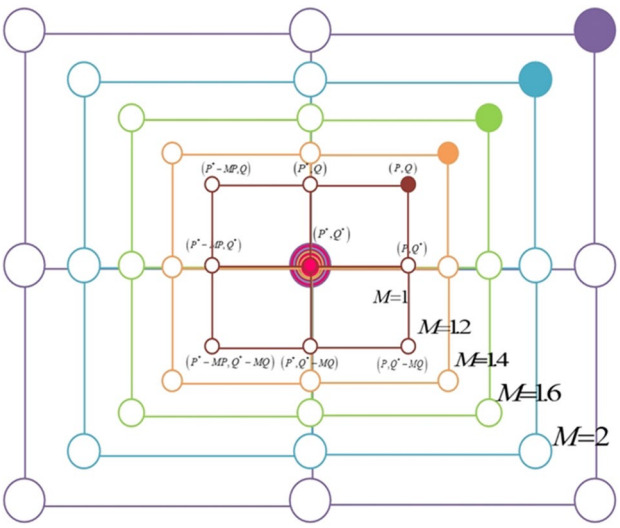

Fig. 4 Exploration mechanism implemented in WOA (Mirjalili and Lewis 2016)

As humpback whales pursue their prey, they navigate along a spiral path, progressively tightening their movements into an encircling motion. To replicate this behavior, the simulation involves a 50% chance of employing the contraction mechanism or spiral model to adjust the whale's position during optimization. The mathematical representation of this model is as follows:

$$\vec{P}(t+1) = \begin{cases} \vec{P}^*(t) - \overrightarrow{M} \cdot \vec{N} if p < 0.5 \\ \overrightarrow{N}' \cdot e^{bl} \cdot cos(2\pi l) + \vec{P}^*(t) if p > 0.5 \end{cases} \tag{39}$$

In Eq. (39), p is a random value in 0 to 1.

Search for prey In the prey predation stage, the random value of $\left|\overrightarrow{M}\right| \ge 1$ is used to force the whale to expand the search range. During this process, the whale's position is updated via a random position. The corresponding mathematical model is as follows:

$$\vec{K} = \left|\vec{R} \cdot \vec{P}_{\text{rand}} - \vec{P}\right| \tag{40}$$

$$\vec{P}(t+1) = \vec{P}_{\text{rand}} - \overrightarrow{M} \cdot \vec{K} \tag{41}$$

where $\vec{P}_{\text{rand}}$ represents the whale position vector randomly determined in the current population. Figure 4 illustrates the feasible positions that can be achieved with varying $\left|\overrightarrow{M}\right| \ge 1$ values.

A set of initial solutions is randomly generated to initiate the WOA algorithm. In each iteration, the whale updates its position according to the randomly selected solution or the current optimal solution. That is, when $\left|\overrightarrow{M}\right| \ge 1$, randomly select a solution to update the whale's position; when $\left|\overrightarrow{M}\right| < 1$, the new location of whales is selected by the current best solution. Meanwhile, **WOA** switches freely between the two mechanisms of spiral position update and shrinking encircling mechanism according to the value of p.

The flowchart of WOA algorithm is shown in Fig. 5(b).

Modeling process of the proposed model

To optimize the background value parameter α and order r in the proposed FBNGM (1, N, r) model, the WOA algorithm is employed. The modeling process of the resulting optimized FBNGM (1, N, r) model is shown in Fig. 5, and further elaborated as follows:

Step 1: Select the characteristic variable sequence and driving variable sequence.

Step 2: Eqs. (3) and (4) are used to calculate the r-AGO sequences $\boldsymbol{Y}^{(r)}$ and $\boldsymbol{X}_k^{(r)}, k = 2, 3, \cdots, N$ with unknown

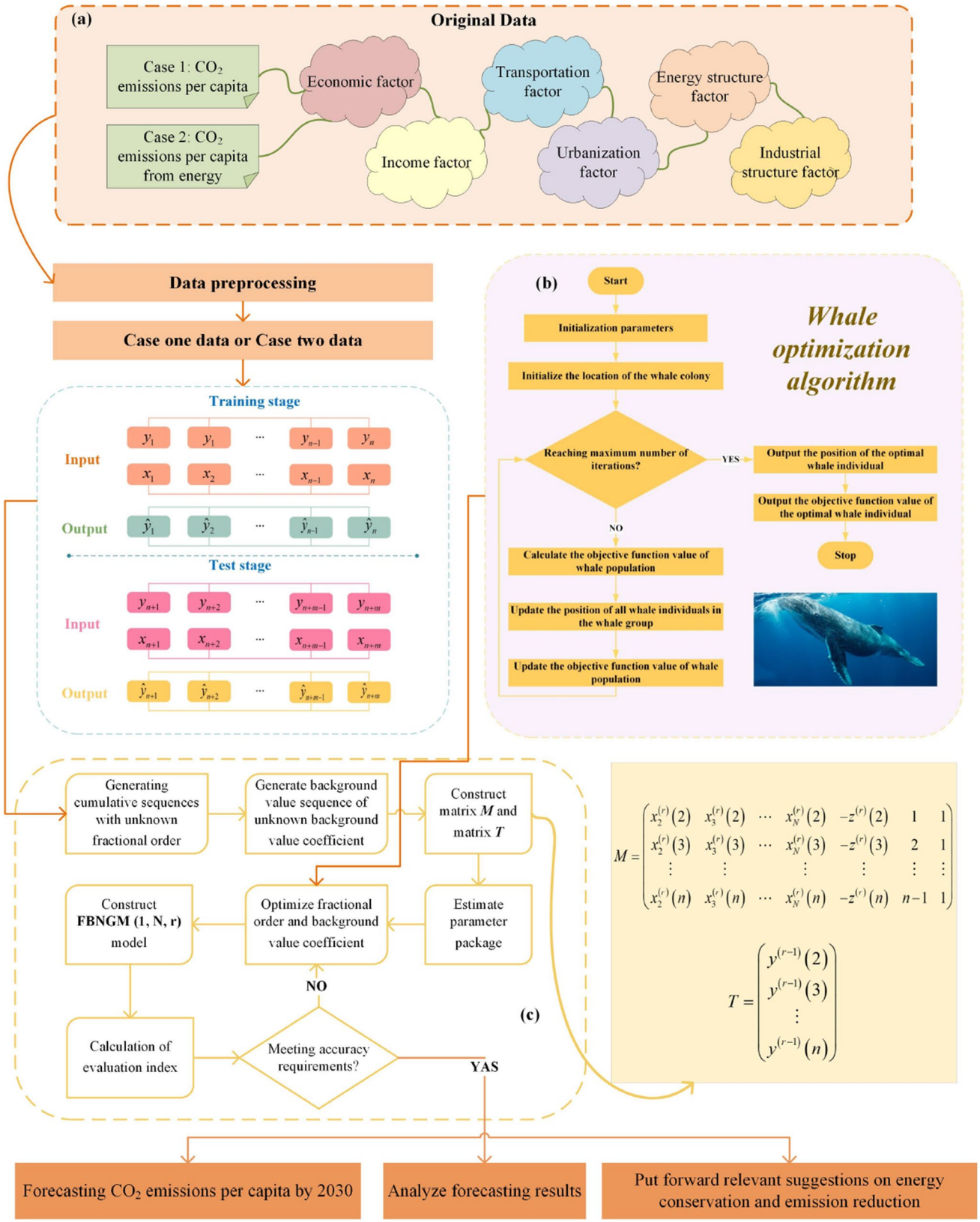

Fig. 5 The flowchart of the proposed grey model in this study

orders r, using Eqs. (5) and (6) to calculate the $(r-1)$ -AGO sequences $\boldsymbol{Y}^{(r-1)}$ and background value sequence $\boldsymbol{Z}^{(r)}$ with unknown fractional order r and background value parameter α.

Step 3: Based on the sequences $\boldsymbol{Y}^{(r)}$, $\boldsymbol{X}_k^{(r)}, k=2,3,\cdots,N$, $\boldsymbol{Y}^{(r-1)}$, and $\boldsymbol{Z}^{(r)}$, the parameter matrices $\boldsymbol{M}$ and $\boldsymbol{W}$ for the FBNGM (1, N, r) model are constructed. Subsequently, the values of each parameter in the parameter vector $\widehat{\boldsymbol{g}}=\left[m_2,m_3,\cdots,m_N,p,q_1,q_2\right]^T$ for the FBNGM (1, N, r) model is estimated given an unknown order r and background value parameter α.

Step 4: Utilizing the WOA algorithm, the parameters r and α are optimized. Based on the obtained optimal values of r and α, the estimated value of each parameter in the parameter vector $\widehat{\boldsymbol{g}}=\left[m_2,m_3,\cdots,m_N,p,q_1,q_2\right]^T$ is calculated, thereby establishing the FBNGM (1, N, r) model.

Step 5: The performance of the FBNGM (1, N, r) model is evaluated in both the training and test sets by calculating metrics such as mean absolute error (MAE), absolute percentage error (APE), mean absolute percentage error (MAPE), and root mean square error (RMSE).

Step 6: If the performance of the FBNGM (1, N, r) model meets the accuracy requirements, the model is used to predict future values. The predicted future values are then analyzed, and relevant policy recommendations and suggestions that can be implemented are proposed based on the analysis.

Table 1 Actual value of total energy consumption, the proportion of coal, petroleum, and natural gas, population, and CO_2 emissions per capita from 1990 to 2022

Year	Total energy consumption (10,000 T)	Proportion of coal (%)	Proportion of petroleum (%)	Proportion of natural gas (%)	Population (billions)	CO_2 emissions (t)
1990	98,703	76.2	16.6	2.1	114,333	2.07
1991	103,783	76.1	17.1	2.0	115,823	2.16
1992	109,170	75.7	17.5	1.9	117,171	2.24
1993	115,993	74.7	18.2	1.9	118,517	2.34
1994	122,737	75.0	17.4	1.9	119,850	2.44
1995	131,176	74.6	17.5	1.8	121,121	2.57
1996	135,192	73.5	18.7	1.8	122,389	2.62
1997	135,909	71.4	20.4	1.8	123,626	2.58
1998	136,184	70.9	20.8	1.8	124,761	2.56
1999	140,569	70.6	21.5	2.0	125,786	2.63
2000	146,964	68.5	22.0	2.2	126,743	2.68
2001	155,547	68.0	21.2	2.4	127,627	2.78
2002	169,577	68.5	21.0	2.3	128,453	3.02
2003	197,083	70.2	20.1	2.3	129,227	3.53
2004	230,281	70.2	19.9	2.3	129,988	4.10
2005	261,369	72.4	17.8	2.4	130,756	4.66
2006	286,467	72.4	17.5	2.7	131,448	5.08
2007	311,442	72.5	17.0	3.0	132,129	5.48
2008	320,611	71.5	16.7	3.4	132,802	5.55
2009	336,126	71.6	16.4	3.5	133,450	5.79
2010	360,648	69.2	17.4	4.0	134,091	6.08
2011	387,043	70.2	16.8	4.6	134,916	6.56
2012	402,138	68.5	17.0	4.8	135,922	6.65
2013	416,913	67.4	17.1	5.3	136,726	6.80
2014	428,334	65.8	17.3	5.6	137,646	6.83
2015	434,113	63.8	18.4	5.8	138,326	6.80
2016	441,492	62.2	18.7	6.1	139,232	6.77
2017	455,827	60.6	18.9	6.9	140,011	6.87
2018	471,925	59.0	18.9	7.6	140,541	6.98
2019	487,488	57.7	19.0	8.0	141,008	7.09
2020	498,314	56.8	18.9	8.4	141,212	7.17
2021	524,000	56.0	18.5	8.9	141,260	7.45
2022	541,000	56.2	17.9	8.4	141,175	7.64

Table 2 Carbon emission factor coefficients from the consumption of three fossil energy sources

Data sources	Coal	Petroleum	Natural gas
Energy Information Administration of the U.S. Department of Energy	0.7020	0.4780	0.3890
Japan Energy Economy Research Institute	0.7560	0.5860	0.4490
Chinese Academy of Engineering	0.6800	0.5400	0.4100
National Environmental Protection Administration Greenhouse Gas Control Project	0.7480	0.5830	0.4440
Climate Change Project of State Science and Technology Commission	0.7260	0.5830	0.4090
Energy Research Institute of National Development and Reform Commission	0.7476	0.5825	0.4435
Mean values	0.7266	0.5588	0.4241

Sources: the data are collected from bulletins and reports from various institutions (Peng et al. 2011)

Model application

In this section, two numerical case studies are performed to assess the efficacy of the newly developed FBNGM (1, N, r) model in predicting CO_2 emissions per capita. To further assess the effectiveness of the FBNGM (1, N, r) model, three univariate grey models (NGM (1, 1), FNGM (1, 1), and FBNGM (1, 1)), two multivariable grey models (NGM (1, N) and FNGM (1, N)), a statistical model MLR, a machine learning model SVR, and a neural network model BPNN are compared the model proposed in this study. Furthermore, APE, MAE, RMSE, and MAPE introduced in "Evaluation criteria" are also utilized to analyze the errors of the nine models established in each case. Additionally, the specific experimental data, model evaluation criteria, and analysis and discussion of the experimental results are described in detail as follows.

Data description

Case 1 adopts CO_2 emissions per capita data collected from the World Bank for model training and testing, and case 2 uses CO_2 emissions per capita data (see Table 1) calculated based on fossil energy consumption data obtained from the China Statistical Yearbook 2021 and carbon emission factor coefficients and carbon emission factors obtained from a combination of research institutes (see Table 2).

According to the setup of the multivariate model of this study, six factors affecting CO_2 emissions are introduced:

(1) Economic: Sustained economic growth is usually accompanied by a high level of energy consumption and extensive resource utilization, which leads to an increase in the emission of large quantities of greenhouse gases, such as CO_2 (Jian et al. 2021). This study selects GDP per capita as the economic factor, referencing existing studies.
(2) Income: In general, as the economic development and per capita income level of a country or region increase, carbon emissions usually increase (Ehigiamusoe and Dogan 2022). Therefore, this study uses the disposable income of residents as an income indicator to introduce the model.
(3) Transportation: With population growth, accelerated urbanization, and economic activities, the demand for transportation is increasing, and transportation involves the use of large amounts of energy, which in turn contributes to the generation of carbon emissions (Jiang et al. 2022). In this study, the volume of goods transported is used as an indicator to reflect transportation.
(4) Urbanization rate: Since urbanization is associated with increased energy demand, transport development, and industrialization, an increase in the rate of urbanization tends to be associated with an increase in carbon emissions (Xiaomin and Chuanglin 2023).
(5) Energy structure: an irrational energy structure will bring great harm to the ecological environment and the physical and mental health of the people, as well as pose a potential threat to the sustainable development of China's economy, therefore, it is crucial to transition to cleaner energy sources and to reduce dependence on fossil fuels (Li et al. 2021b). The proportion of clean energy is selected in this study as an indicator of energy structure.
(6) Industrial structure: China's industrialization is accelerating, and the secondary industry, which is high in energy consumption and pollution, is the main source of CO_2 emissions, and the adjustment of industrial structure has an important impact on emission reduction (Wang et al. 2019). In this study, the proportion of added value of the secondary industry in GDP is included in the prediction model of CO_2 emission as an influential factor to measure the industrial structure.

Except for the CO_2 data, all the other data have been obtained from the National Bureau of Statistics of China. For the first case study, annual CO_2 emissions per capita data from 1990 to 2020 are collected and divided into two sets: the training set (1990–2016) and the test set (2017–2020). The training set is used to build the model, and

its performance is evaluated by applying the model to the test set. The training set for the second case study is the years 1990 to 2015, while the data as the test set used to evaluate performance in the model spans the years 2016 to 2022.

Data processing

This study converts fossil fuel consumption into CO_2 emissions per capita, as CO_2 emissions are closely linked to the consumption of fossil fuels. To achieve this, the consumption of each fossil fuel type is calculated by considering the total energy consumption and the proportion of different fossil fuel sources. Specifically, the consumptions of coal, oil, and natural gas are determined using the following formula:

$$\boldsymbol{EC}_i = \boldsymbol{E} \times k_i, i = 1, 2, 3 \tag{42}$$

where $\boldsymbol{E}$ is the total energy consumption. $\boldsymbol{EC}_i(i = 1, 2, 3)$ represents the corresponding consumption of coal, oil, and natural gas, respectively. $k_i(i = 1, 2, 3)$ represents the proportion of coal, oil, and natural gas, respectively. All data are listed in Table 1.

Second, the CO_2 emissions are determined using the calculation formula from the Intergovernmental Panel on

Table 3 The evaluation criteria for model performance

Indicator	Abbreviation	Formula
Mean absolute error	**MAE**	$\boldsymbol{MAE} = \frac{1}{n}\sum_{i=1}^{n}\lvert e(i)\rvert$
Absolute percentage error	**APE**	$\boldsymbol{APE}(i) = \left\lvert \frac{e(i)}{y^{(0)}(i)} \right\rvert \times 100\%$
Mean absolute percentage error	**MAPE**	$\boldsymbol{MAPE} = \frac{1}{n}\sum_{i=1}^{n}\boldsymbol{APE}(i)$
Root mean square error	**RMSE**	$\boldsymbol{RMSE} = \sqrt{\frac{1}{n}\sum_{i=1}^{n}\left(e^2(i)\right)}$

$e(i) = \hat{y}^{(0)}(i) - y^{(0)}(i)$ is the ith residual error, $y^{(0)}(i)$ represents the ith real data, and $\hat{y}^{(0)}(i)$ is the ith predicted value

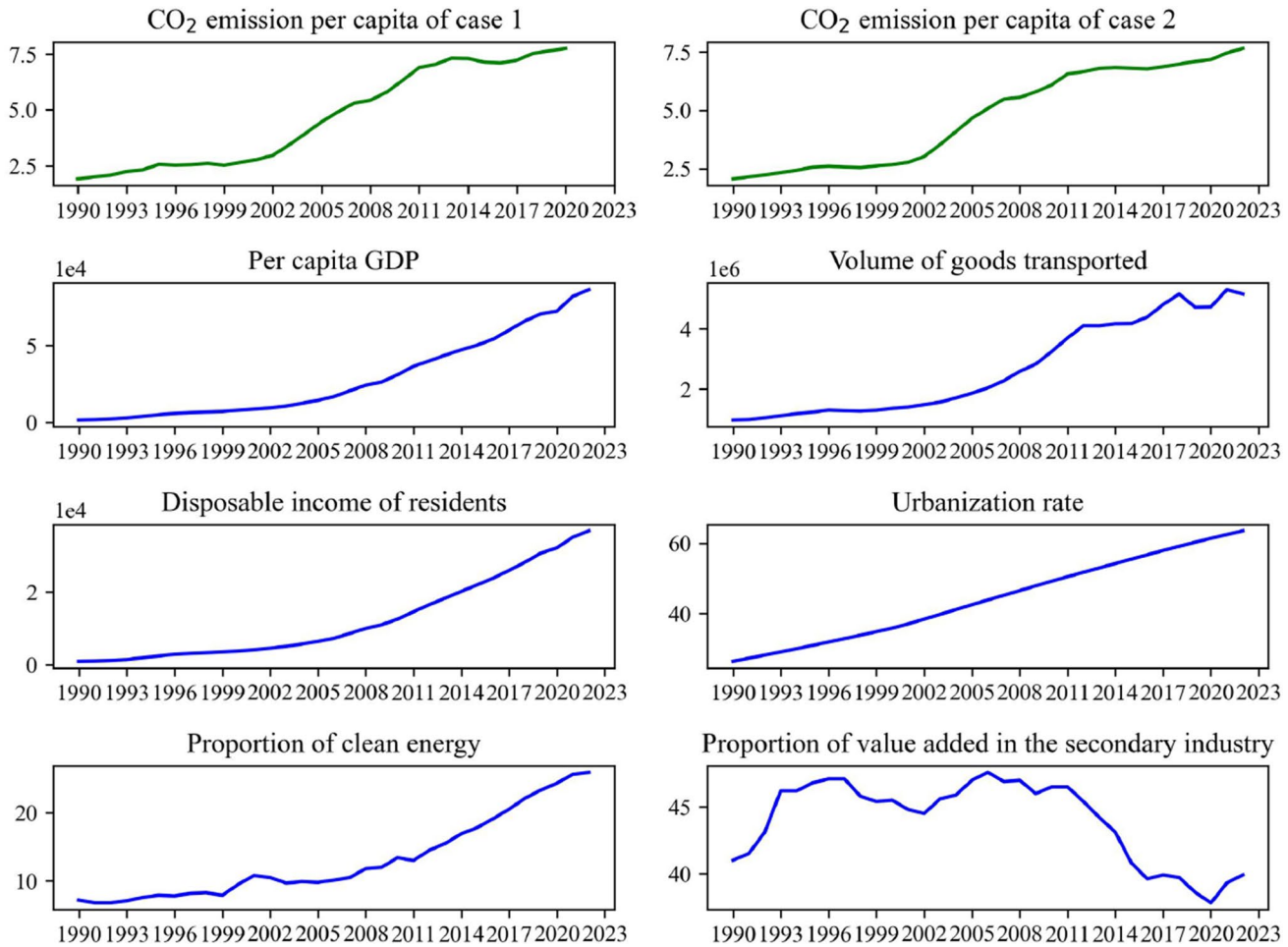

Fig. 6 All data visualizations

Table 4 Benchmark of modelling accuracy evaluation level about MAPE (Zhou et al. 2020)

Evaluation index	Prediction performance			
	Poor	Medium	Good	Excellent
MAPE (%)	> 50	20–50	10–20	< 10

Climate Change (IPCC). The equation used for this calculation is as follows:

$$\boldsymbol{CE} = \sum \boldsymbol{EC}_i \times \boldsymbol{EF}_i \times \frac{44}{12} \tag{43}$$

In Eq. (43), $\boldsymbol{CE}$ means CO_2 emissions, $\boldsymbol{EF}_1, \boldsymbol{EF}_2, \boldsymbol{EF}_3$ represent the CO_2 emissions factors corresponding to coal, oil, and natural gas, respectively. Among them, the value of $\boldsymbol{EC}_i (i = 1, 2, 3)$ determined by studying the literature. Then, the CO_2 emissions coefficients measured by the six institutions are averaged, as shown in Table 2.

Then, the CO_2 emissions per capita can be calculated according to the following equation.

$$\boldsymbol{PCE} = \boldsymbol{CE}/\boldsymbol{P} \tag{44}$$

where, $\boldsymbol{PCE}$ is CO_2 emissions per capita, and the $\boldsymbol{P}$ is the number of permanent residents at the end of the year. See Table 1 for calculation results. A visualization of the data trends for CO_2 emissions per capita and all influencing factors for both cases is shown in Fig. 6.

Finally, the CO_2 emissions per capita and all influencing factors data in the two cases are standardized by the following formula to eliminate their different dimensions.

$$\boldsymbol{y}_1^{(0)}(i) = \frac{y^{(0)}(i)}{y^{(0)}(1)}, i = 1, 2, \cdots, n \tag{45}$$

$$\boldsymbol{x}_{k1}^{(0)}(i) = \frac{x_k^{(0)}(i)}{x_k^{(0)}(1)}, i = 1, 2, \cdots, n, k = 2, 3, \cdots, N \tag{46}$$

Evaluation criteria

To appraise the precision of the proposed model's predictions, this study employs four criteria: mean absolute error (**MAE**) (Yang et al. 2024), absolute percentage error (**APE**), mean absolute percentage error (**MAPE**) (Cai et al. 2023), and root mean square error (**RMSE**) (Zhao et al. 2022). Table 3 provides a breakdown of each of these criteria and their associated abbreviations. Additionally, Table 4 outlines the classification system used for the model grade based on the **MAPE**.

Case study 1 — China's CO_2 emissions per capita from the World Bank

For this subsection, CO_2 emissions per capita data from the World Bank spanning the decade of 1990 to 2020 is used. Specifically, data from 1990 to 2017 is utilized to construct the model, while data from 2018 to 2020 is reserved for testing the model's performance.

Empirical calculation and results

According to the modeling steps and flowchart introduced in "Modeling process of the proposed model", the CO_2 emissions per capita ($\boldsymbol{Y}^{(0)}$) of the research object and the influencing factors GDP per capita ($\boldsymbol{X}_2^{(0)}$), volume of goods transported ($\boldsymbol{X}_3^{(0)}$), disposable income of residents ($\boldsymbol{X}_4^{(0)}$), urbanization rate ($\boldsymbol{X}_5^{(0)}$), proportion of clean energy ($\boldsymbol{X}_6^{(0)}$), and proportion of added value of the secondary industry ($\boldsymbol{X}_7^{(0)}$) are brought into the optimized FBNGM (1, N, r) model, and the optimized fractional order and background value coefficients are obtained as follows:

$$r = 0.7730, r_2 = 0.9246, r_3 = 0.1460, r_4 = 0.8579,$$
$$r_5 = 0.0212, r_6 = 0.7449, r_7 = 0.9492, \xi = 0.5113$$

Thus, the parameter vector $\hat{\boldsymbol{g}}$ of the model can be obtained and further the time response equation of the FBNGM (1, N, r) model can be obtained:

Table 5 Comparison of the prediction accuracies of the six models

Model	Training stage			Test stage		
	MAPE (%)	MAE	RMSE	MAPE (%)	MAE	RMSE
NGM (1, 1)	10.81	0.41	0.47	15.27	1.17	1.19
FNGM (1, 1)	10.09	0.42	0.53	3.29	0.25	0.28
FBNGM (1, 1)	9.46	0.43	0.55	1.94	0.15	0.19
NGM (1, N)	4.19	0.16	0.20	26.47	2.04	2.30
FNGM (1, N)	1.33	0.05	0.07	8.58	0.66	0.74
FBNGM (1, N, r)	**1.29**	**0.05**	**0.07**	**0.61**	**0.05**	**0.06**
MLR	3.55	0.13	0.16	5.13	0.39	0.43
SVR	5.86	0.21	0.23	26.16	2.01	2.08
BPNN	2.29	0.08	0.11	14.51	1.12	1.27

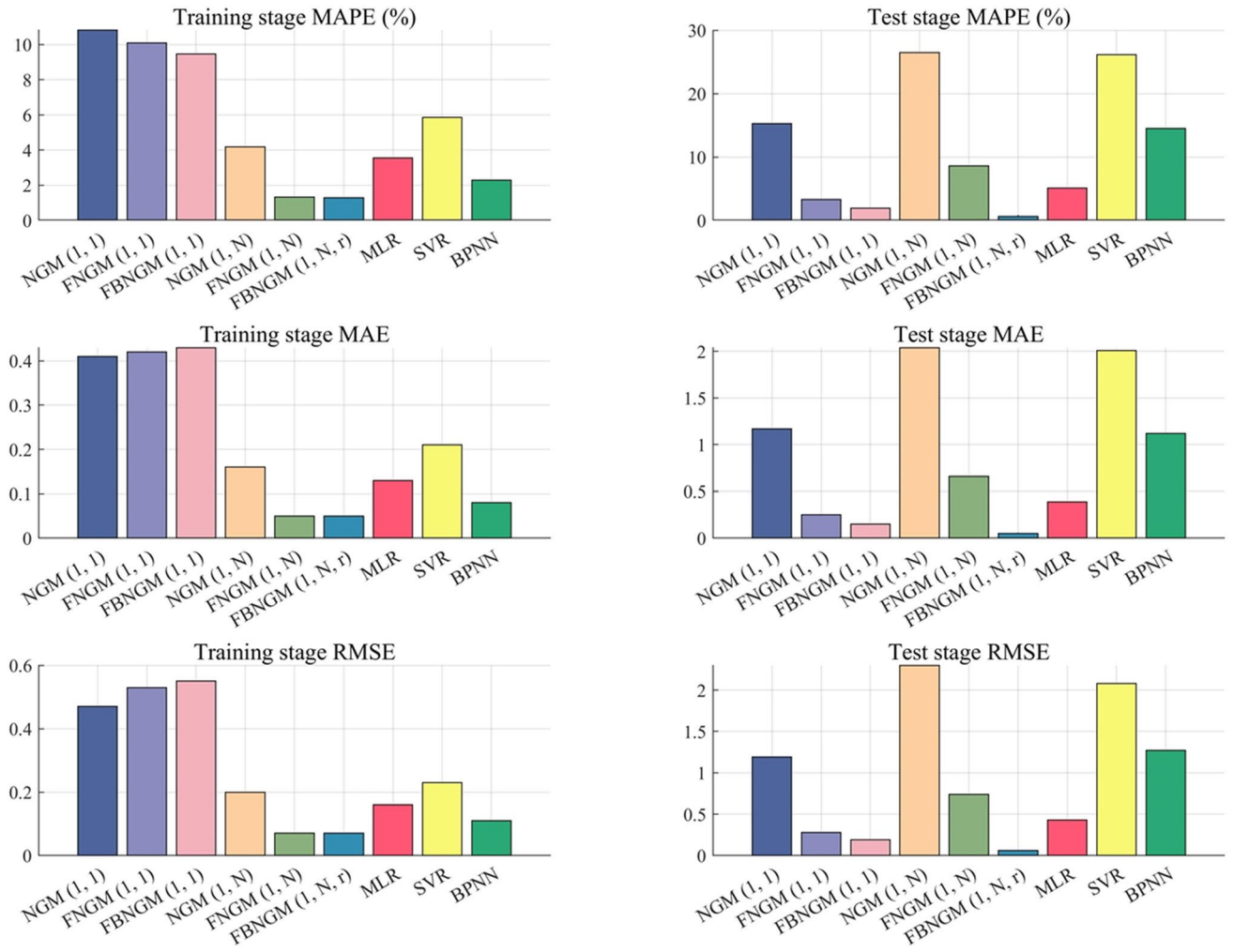

Fig. 7 Comparison of evaluation criteria for case 1

$$\hat{g} = [0.1267, -0.0579, -0.1318, 21.6486, -0.2111, 1.8964, 0.5457, -2.3449, -22.1811]^T$$

$$\hat{y}^{(0)}(i) = y^{(0)}(1) \times \sum_{t=0}^{i-1} (-1)^t \frac{\Gamma(0.7730+1)}{\Gamma(t+1)\Gamma(0.7730-t+1)} \left\{ \sum_{u=1}^{i-1} \left[0.7818 \times \sum_{k=2}^{N} 0.5733^{u-1} \times \left(0.1267 \times x_2^{(r)}(i-u+1) - 0.0579 \times x_3^{(r)}(i-u+1) - 0.1318 \times x_4^{(r)}(i-u+1) + 21.6486 \times x_5^{(r)}(i-u+1) - 0.2111 \times x_6^{(r)}(i-u+1) + 1.8964 \times x_7^{(r)}(i-u+1) \right) \right] + 0.5733^{i-1} \hat{y}^{(r)}(1) + \sum_{j=0}^{i-2} 0.5733^j \left[-1.8333(i-j) - 15.5088 \right] \right\}$$

Forecasting performance evaluation

To illustrate the efficacy of the proposed model, this has been evaluated by comparing with two multivariate models (NGM (1, N), FNGM (1, N)), three univariate models (NGM (1, 1), FNGM (1, 1), and FBNGM (1, 1)), a statistical model (MLR), a machine learning model (SVR), and a neural network model (BPNN). The findings for each evaluation criterion are presented in Table 5, which is based on the assessment of the accuracy and performance of all nine models using the criteria in the "Evaluation criteria." An intuitive way to assess the performance and accuracy of various approaches is to create bar charts. Figure 7 displays the comparison chart. Figure 8 shows a box plot of the APE indicator. Additionally, Fig. 9 shows the curves produced by the

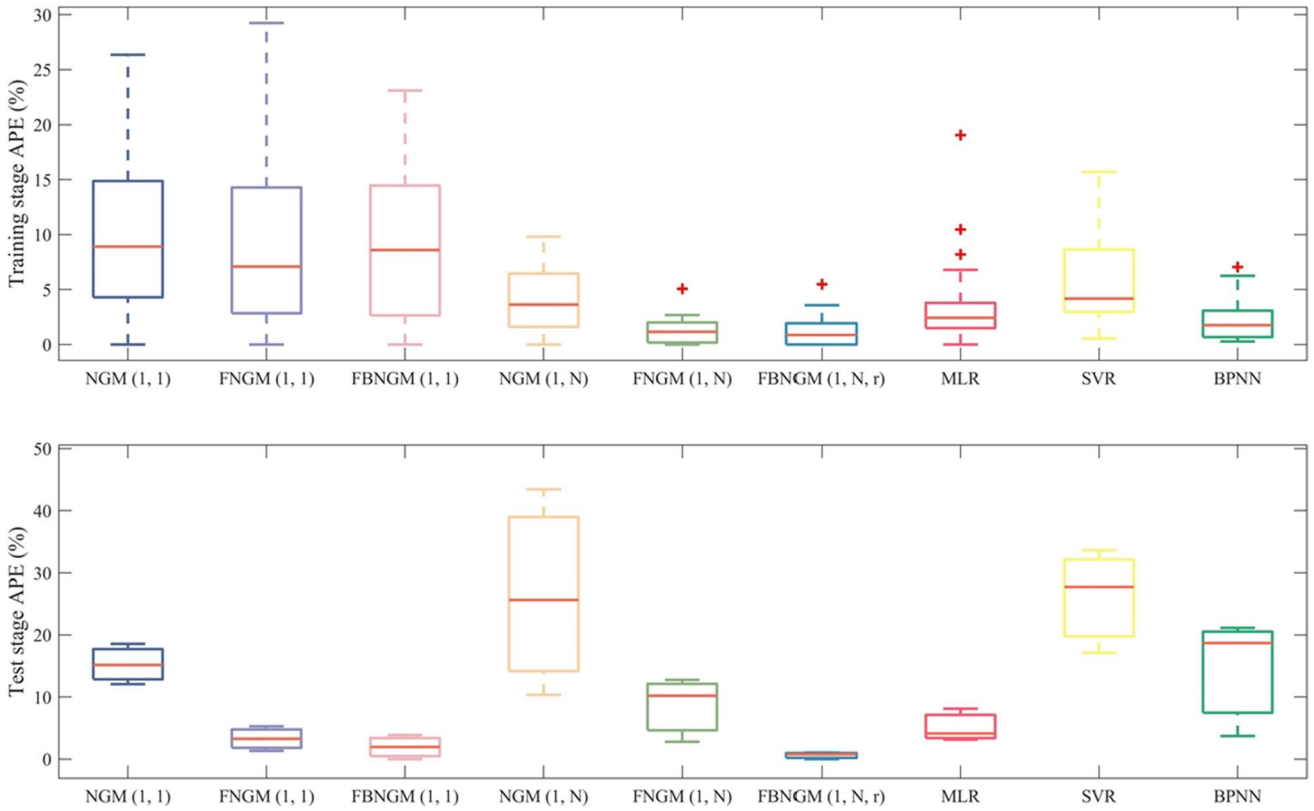

Fig. 8 Comparison of APE results for the nine models in case 1

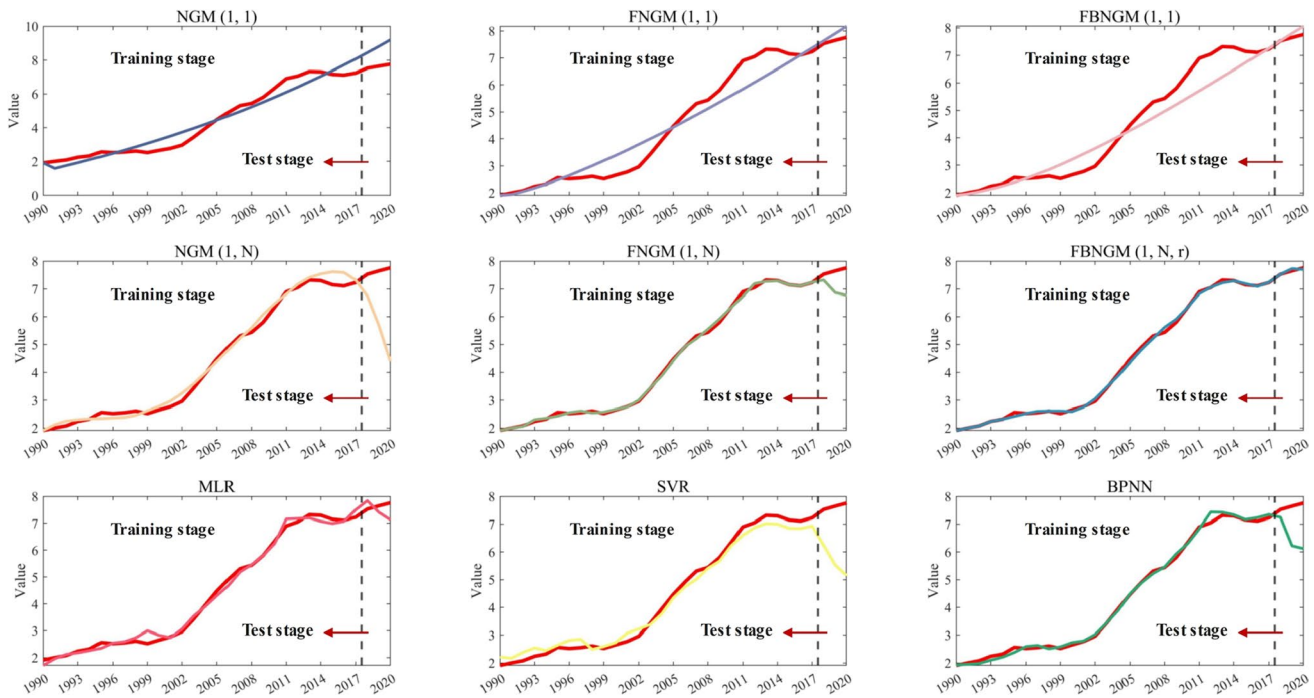

Fig. 9 Comparison of the observed and simulated values of the nine models for case 1

various models that represent the expected values and matching observed values. In addition, the experimental data will undergo three comparisons: (1) a comparison between the proposed model and univariate grey models; (2) a comparison between the proposed model and multivariate grey models; and (3) a comparison between the proposed model and non-grey models.

(1). For the univariate grey prediction model, the original model, NGM (1, 1), obtained the worst prediction results in both the training and test stages (10.81% and 15.27%, respectively). Although its MAE and RMSE values in the training stage are lower than the other two univariate grey prediction models, the MAPE value is the highest and the NGM (1, 1) model is the only univariate model with a MAPE value higher than 10% in the test stage. The FBNGM (1, 1) model is the only model with a MAPE value lower than 10% in the training stage (MAPE = 9.46%) and achieved the best prediction results in the test stage (MAPE = 1.94%). In addition, the accuracy of the NGM (1, 1) model in the training phase is higher than the accuracy in the test phase, suggesting that the model produced an overfitting phenomenon, which is avoided by the model proposed in this study.

In terms of APE value distribution, as shown in Fig. 8, the APE values of the NGM (1, 1), FNGM (1, 1), and FBNGM (1, 1) models in the training phase span from 0.45 to 26.35%, 0.00 to 29.24%, and 0.00 to 23.10%, respectively. The APE values of the three models in the testing phase span from 12.08 to 18.56%, 1.33 to 5.28%, and 0 to 3.87%, and it is clear that the FBNGM (1, 1) model proposed in this study performs best on case 1.

The results show that the fractional order model FBNGM (1, 1) proposed in this study with optimized background value coefficients fits and predicts best for case 1 in the univariate model.

(2). For the multivariate grey prediction models, it can be obtained from Table 5 and Fig. 7 that the accuracies of the three multivariate grey prediction models are higher than the univariate grey prediction models in the training stage, which indicates that the influences added in this study are effective and enhance the prediction effect of the models. For the evaluation index MAPE, FBNGM (1, N, r) has a value of 1.29% in the training stage, which is 2.9% higher than the NGM (1, N) model and 0.04% higher than the FNGM (1, N) model, while in the testing stage, the prediction accuracy of the FBNGM (1, N, r) model is 0.61%, which is 7.97% and 25.86% higher than the other two multivariate grey prediction models, respectively. For the indicators MAE and RMSE, although the FBNGM (1, N, r) model and the FNGM (1, N) model have the same results in the testing stage, the FBNGM (1, N, r) model reflects a clear advantage in the testing stage.

For the APE metrics that respond to the distribution of errors, according to the box-and-line diagram in Fig. 8, it can be obtained that in the training stage, the distributions of the FNGM (1, N) and FBNGM (1, N, r) models are the same, while the error fluctuation of the NGM (1, N) model is more drastic. However, it is clear that the FBNGM (1, N, r) model has the smallest error fluctuation in the testing phase, and the accuracy of the model is significantly better than that of the FNGM (1, N) and NGM (1, N) models.

It follows that effective influences improve the accuracy of the model. The fractional order cumulative operator can better mine the data trend, and the optimized background value coefficient can further improve the accuracy of the model.

(3). For the non-grey models (MLR, SVR, and BPNN), it can be seen from Table 5 and Fig. 7 that all three models achieved superior prediction accuracy in the training phase, whereas only the MLR model had a prediction accuracy of less than 10% in the testing phase. BPNN is the best-performing non-grey model in the training phase (MAPE = 2.29%) and MLR is the best-performing non-grey model in the testing phase (MAPE = 5.13%). However, the non-grey model accuracy is significantly lower compared to the 1.29% and 0.61% of the FBNGM (1, N, r) model proposed in this study. The low accuracy of the machine learning model SVR and the neural network model BPNN can be attributed to the small amount of data, which is insufficient for model training. Although the amount of data may satisfy the requirements of statistical modeling, the accuracy is still not as good as the model proposed in this study.

In terms of error distribution, the accuracy of the non-grey model, which integrates multiple influencing factors, is higher than that of the non-grey model in the training phase despite the sparser data. The accuracies of the multivariate grey prediction models, except for the NGM (1, N) model, are higher than those of the machine learning model SVR and the neural network model BPNN in the testing stage. The accuracy of the non-grey model is not as good as most of the grey prediction models in the testing stage, but in general, the model proposed in this study achieves the highest accuracy.

Based on the above analysis, it can be concluded that the FBNGM (1, N, r) model proposed in this study can fully mine the data information and avoid the phenomenon of overfitting. In addition, from the prediction results in Fig. 9, the fitting and prediction effects of the FBNGM (1, N, r) model are closer to the real data.

Table 6 Comparison of the prediction accuracies of the six models

Model	Training stage			Test stage		
	MAPE (%)	MAE	RMSE	MAPE (%)	MAE	RMSE
NGM (1, 1)	9.10	0.32	0.36	37.33	2.69	2.88
FNGM (1, 1)	8.28	0.31	0.38	17.19	1.24	1.32
FBNGM (1, 1)	8.26	0.31	0.38	17.90	1.29	1.38
NGM (1, N)	64.19	4.01	8.17	2319.44	169.16	208.24
FNGM (1, N)	1.29	0.05	0.06	2.49	0.18	0.26
FNGM (1, N, r)	**1.04**	**0.04**	**0.05**	**1.38**	**0.10**	**0.12**
MLR	4.51	0.15	0.20	5.32	0.39	0.54
SVR	6.69	0.33	0.43	42.89	3.05	3.07
BPNN	7.44	0.31	0.36	6.32	0.46	0.64

The values of the individual evaluation metrics of the NGM (1, N) model are not shown in this figure due to their excessive size

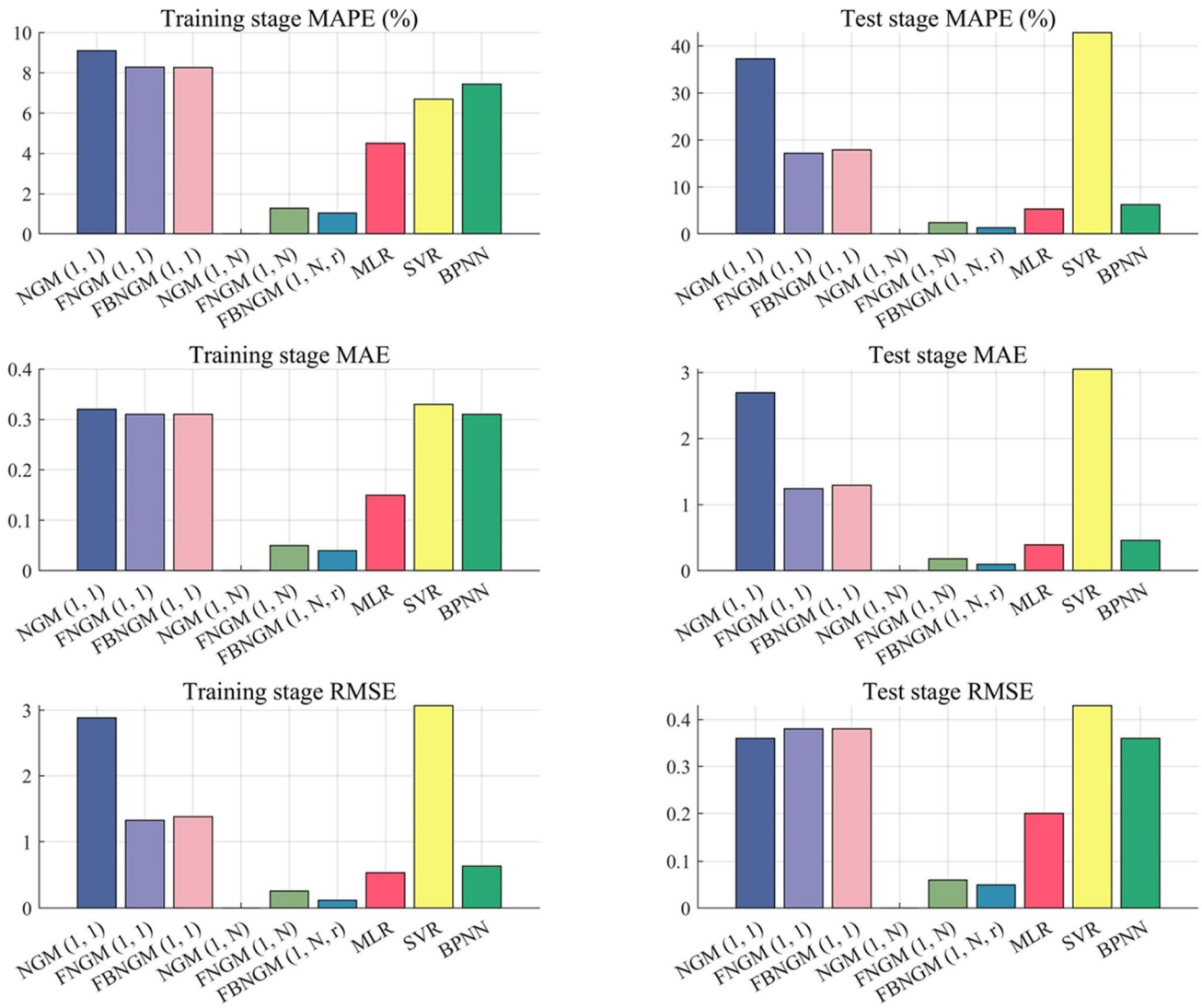

Fig. 10 Comparison of evaluation criteria for case 2. Note: The NGM (1, N) model is not shown in this figure because the error fluctuations are too large

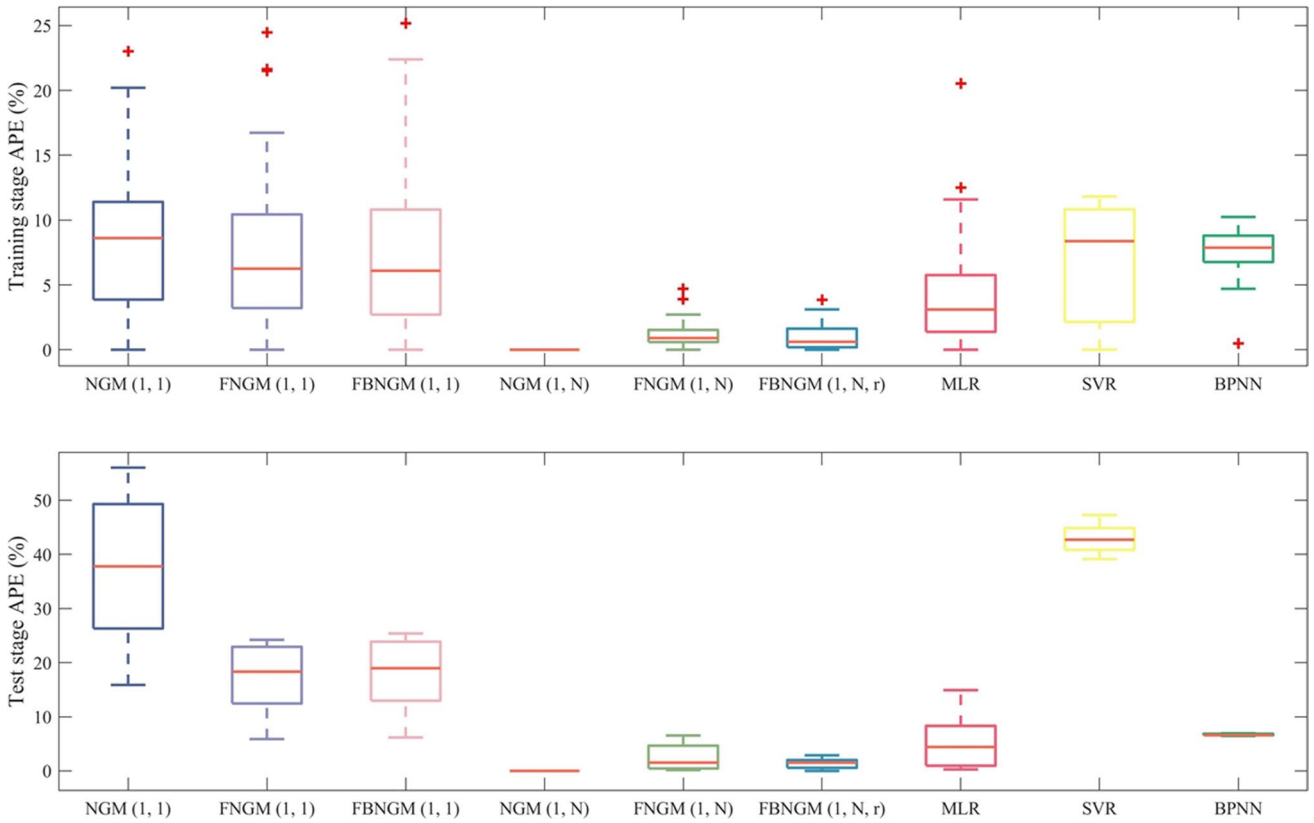

Fig. 11 Comparison of APE results for the nine models in case 2

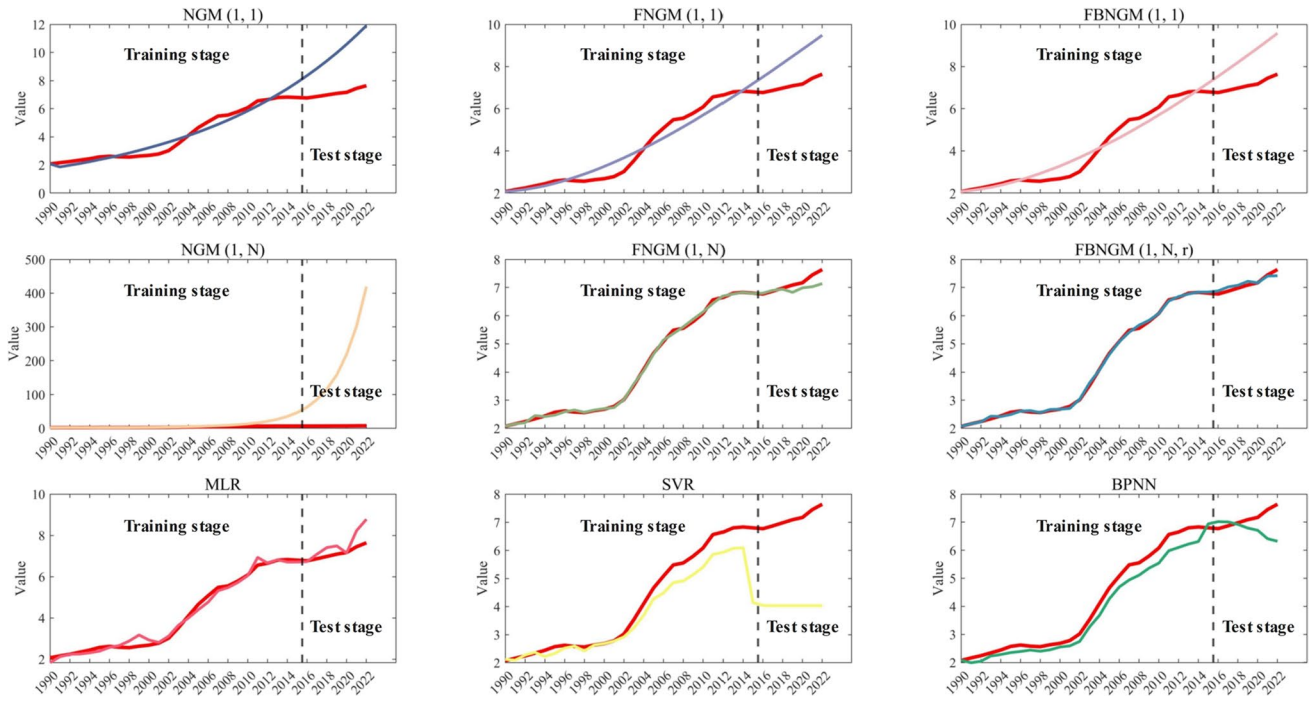

Fig. 12 Comparison of observed and simulated values of the six models

Case study two — CO_2 emissions per capita calculated from the energy data

For this section, the statistics on energy and influencing factors from 1990 to 2022 are chosen, and the CO_2 emissions per capita from energy are computed using the technique described in "Data processing." The data between 1990 and 2015 are used for modeling, while the data between 2016 and 2022 are kept for testing.

Empirical calculation and results

According to the procedure in "Modeling process of the proposed model," the fractional order for the study object and each influencing factor and background value coefficient of the FBNGM (1, N, r) model in case two are as follows:

$$r = 0.8650, r_2 = 0.9871, r_3 = 0.7953, r_4 = 0.5114,$$
$$r_5 = 0.9898, r_6 = 0.5955, r_7 = 0.6531, \xi = 0.4931$$

Then, the parameter vector $\hat{\boldsymbol{g}}$ can be received:

$$\hat{\boldsymbol{g}} = [-0.0751, -0.0319, 0.2388, 3.0528, -0.5238, 3.0247, 0.8787, -4.0098, -4.3738]^T$$

The time-response expression of the FBNGM (1, N, r) can be expressed by

$$\begin{aligned}\hat{y}^{(0)}(i) = y^{(0)}(1) \times \sum_{t=0}^{i-1} (-1)^t \frac{\Gamma(0.8650+1)}{\Gamma(t+1)\Gamma(0.8650-t+1)} \Bigg\{ \sum_{u=1}^{i-1} \Bigg[1.0400 \times \sum_{k=2}^{N} 1.3800^{u-1} \times \\ \Big(-0.0751 \times x_2^{(r)}(i-u+1) - 0.0319 \times x_3^{(r)}(i-u+1) - 0.2388 \times x_4^{(r)}(i-u+1) \\ +3.0528 \times x_5^{(r)}(i-u+1) - 0.5238 \times x_6^{(r)}(i-u+1) + 3.0247 \times x_7^{(r)}(i-u+1) \Big) \Bigg] \\ +1.3800^{i-1} \hat{y}^{(r)}(1) + \sum_{j=0}^{i-2} 1.3800^j \left[-2.7976(i-j) - 0.2540 \right] \Bigg\}\end{aligned}$$

Table 6 presents the calculated evaluation metrics for the **MAE**, **MAPE**, and **RMSE** indexes. Correspondingly, Fig. 10 visualizes the results of the evaluation indicators.

Forecasting performance evaluation

To thoroughly investigate the applicability of the proposed model FBNGM (1, N, r), several other prediction models are included in the comparison. These models consist of three univariate grey prediction models, two multivariate grey prediction models, and three non-grey prediction models. The performance of all nine models is assessed using the metrics described in "Evaluation criteria." Histograms of the evaluation metrics are plotted for both the training and test phases, as shown in Fig. 10. Additionally, box plots of the APE values are generated to examine error fluctuations (Fig. 11), and comparisons between simulated and actual values are shown in the form of curves (Fig. 12). The following discussion will provide an analysis of the results obtained from both the training and test phases.

Regarding the training phase, the NGM (1, N) model demonstrated the poorest performance, with a MAPE value of 64.19%. This value is 63.15% higher than the model proposed in this study, which exhibited the highest accuracy. The performance in the metrics MAE and RMSE is still the worst for the NGM (1, N) model. And for the multivariate grey prediction model with added influencing factors and non-grey prediction model except NGM (1, N) have higher accuracy than the univariate grey prediction model, which indicates that the NGM (1, N) model fails to mine all the information of the data. From Fig. 10, the FBNGM (1, N, r) model proposed in this study performs better than the other two multivariate models and the non-grey prediction model in three indicators. In addition, from Fig. 11, the largest error fluctuations are univariate prediction models in addition to

Table 7 The predicted CO_2 emissions per capita from 2021 to 2030 in case 1 and from 2023 to 2030 in case 2 (unit: t)

Year	CO_2 emissions per capita	
	Case 1	Case 2
2021	8.17	
2022	8.80	
2023	9.09	7.24
2024	9.35	7.14
2025	9.60	7.03
2026	9.86	6.91
2027	10.11	6.75
2028	10.37	6.56
2029	10.61	6.34
2030	10.84	6.08

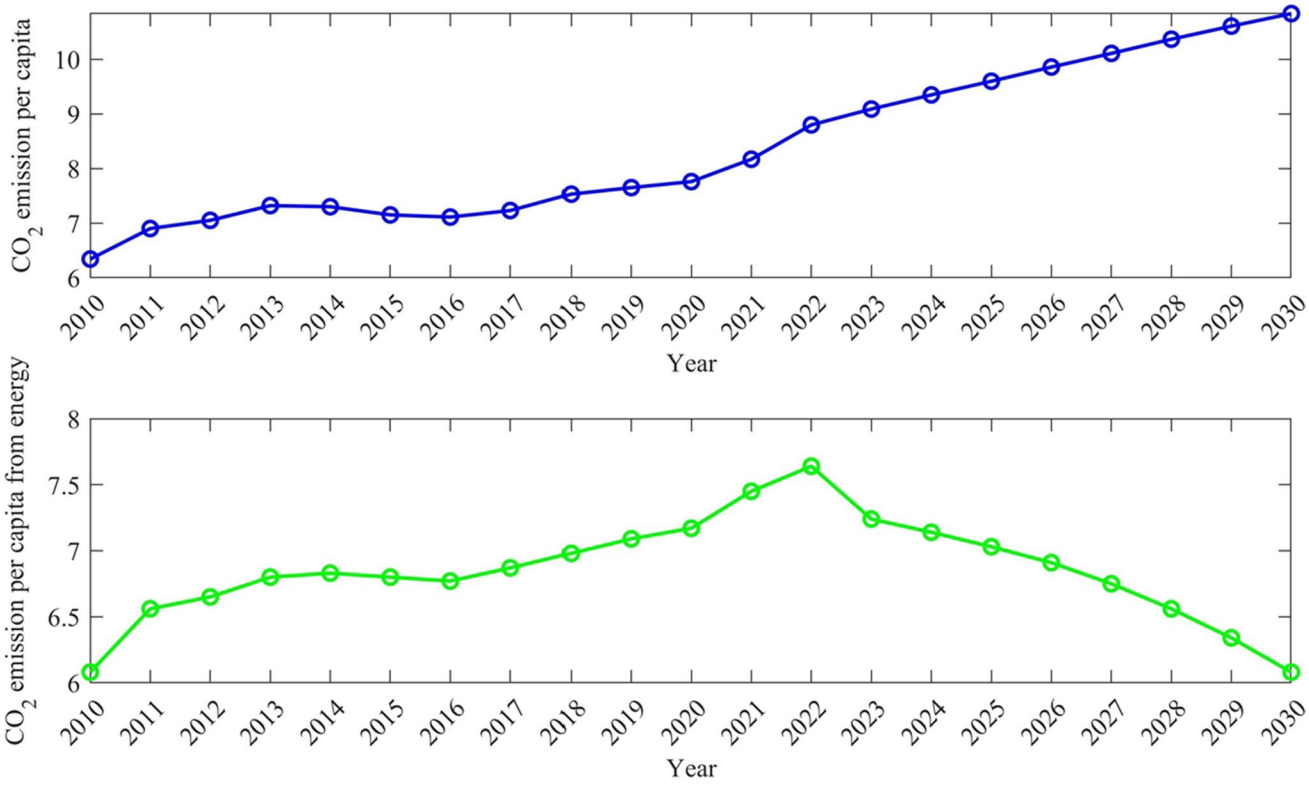

Fig. 13 Future trends in CO_2 emissions per capita

the NGM (1, N) model, which suggests that the influencing factors chosen in this study enhance the prediction accuracy of the model.

As for the discussion of the test stage, only four models, FNGM (1, N), FBNGM (1, N, r), MLR, and BPNN, have MAPE values below 10%, which are 2.49%, 1.38%, 5.32%, and 6.32%, respectively. The MAPE values for the univariate models all exceeded 10%, indicating the crucial role of the influencing factors in predicting CO_2 emissions per capita. From Fig. 10, the best-performing model in terms of MAPE, MAE, and RMSE is the FBNGM (1, N, r) model proposed in this study. Further, from Fig. 11, we can conclude that except for the worst-performing NGM (1, N) model, the NGM (1, 1) model has the largest error fluctuation, which leads to the conclusion that the NGM (1, N) model performs poorly in both univariate and multivariate prediction. The SVR model also displayed suboptimal performance, which may be attributed to the sparse data.

Based on the above comparison of the accuracy of the models in the training and test phases and the comparison curves between the predicted and observed values in Fig. 11, it can be concluded that the FBNGM (1, N, r) model proposed in this study performs optimally among all the models, including univariate grey prediction model, multivariate grey prediction model, and non-grey prediction model.

Forecasting the future CO_2 emissions

After conducting a thorough analysis and rigorous comparison, the FBNGM (1, N, r) model developed in this study has emerged as the most effective tool for predicting CO_2 emissions per capita. Utilizing the FBNGM (1, 1) model, we forecast the influencing factors from 2022 to 2030 and employed Eq. (33) to predict the CO_2 emissions per capita for case 1 from 2021 to 2030 and case 2 from 2022 to 2030. The results of these projections are presented in Table 7.

The prediction results given in Table 7, and the future emission trends shown in Fig. 13 indicate that based on World Bank data, CO_2 emissions per capita are expected to continue to show an upward trend in the coming years. However, emission projections based on energy data from the National Bureau of Statistics of China show a downward trend in CO_2 emissions per capita from energy. The results of this projection can guide the relevant authorities in formulating effective planning.

Discussion and policy suggestions

As people's consumption level continues to grow, CO_2 emissions are gradually becoming a major contributor to the acceleration of global warming. First of all, according to

the Kuznets Environmental Curve (EKC) hypothesis, GDP per capita is closely related to CO_2 emissions (Aslam et al. 2021). The IPCC has implied in the early years that one of the effective ways to reduce the rate of global warming is to change the consumption level of the people (Luo et al. 2023). Secondly, China's growing economic level is closely related to the consumption of large amounts of fossil energy. According to statistics, more than 80% of China's primary energy consumption relies on fossil energy, which directly or indirectly emits large amounts of greenhouse gases (Li and Haneklaus 2021). More importantly, in the context of China's coal-based economy, this has important implications for national development, environmental improvement, and energy security (Lin and Zhu 2019).

According to the proposed FBNGM (1, N, r) model, the CO_2 emissions per capita of the two cases by 2030 can be obtained. Based on the projected CO_2 emissions per capita by 2030 as demonstrated in Table 7 and Fig. 13, the following conclusions can be drawn: first, CO_2 emissions per capita from energy will start to decline from 2023, indicating that China's policy measures in promoting clean energy use and reducing fossil energy consumption have been effective; second, although CO_2 emissions per capita from energy will decline in the future, the combined CO_2 emissions per capita will continue to rise, making it difficult to reach the peak in 2030. The study by Wang et al. (2019) also suggests that current energy efficiency and emission reduction measures and policies may not be sufficient to support the goal of peaking carbon emissions by 2030. Wu and Xu's (2022) study also argues that some regions will not reach the peak by 2030. The study also suggests that China's energy efficiency and emission reduction policies may not be sufficient to support the goal of peaking carbon emissions by 2030. The reason for this situation is that, in addition to CO_2 emissions from energy, CO_2 emissions from transportation, industrial production, and other sources have not been effectively controlled. Therefore, more relevant national and local emission reduction policies need to be put in place to achieve the target. Here are some suggestions given in this study:

(1) Improving the low-carbon development policy system (Wang et al. 2021). The government should exercise its leading role in driving progress towards a greener future. This can be achieved by enhancing the existing green system, which encompasses energy conservation, environment protection, and low-carbon standards, in addition to establishing low-carbon entities such as hospitals, campuses, and institutions (Dalla Longa et al. 2022). In order to promote energy conservation and emission reduction, regulations must be put in place to gradually phase out energy consumption patterns that are detrimental to these goals. Policies relating to energy conservation and emission reduction should also be improved, to foster a more environmentally friendly development paradigm (Huang et al. 2022b).
(2) In order to reduce carbon emissions, it is imperative that we encourage the greater adoption of clean energy sources in place of coal consumption (Gyamfi et al. 2021). As such, we must expedite the development of non-fossil energy and promote the widespread use of clean energy alternatives like wind and solar power. At present, China's main energy consumption is still concentrated in non-clean energy such as coal and oil (Li et al. 2020). Relevant policy makers should pay close attention to it and formulate appropriate policies.
(3) The optimal restructuring of industry represents a crucial means of achieving energy conservation and emission reduction goals. Carbon emissions and industrial structure interact with each other (Zhang et al. 2020). Manufacturing, industry and construction are the main areas that generate carbon emissions (Shan et al. 2020). To achieve our energy conservation and emission reduction objectives, we must undertake efforts to promote the low-carbon transformation of conventional industries and work towards the development of a new green, low-carbon economy. This can be accomplished through industrial restructuring and upgrading, wherein clean energy solutions progressively supplant fossil fuels. By reducing industrial energy consumption and carbon emissions, we can accelerate our transition towards a greener and more sustainable future.
(4) Reducing carbon emissions in human consumption. On the premise of not lowering the living standard, there is a huge space for saving energy for residents (Wang et al. 2020). People are encouraged to travel low-carbon, take more public transport, and reduce the number of private cars. To conserve energy and reduce emissions, we must mindfully utilize electricity, fuel, and solar energy in our daily lives.
(5) The recovery and reuse of renewable resources during the initial production process have the potential to significantly decrease carbon emissions (Chen et al. 2022b). For example, waste iron, battery recycling, garbage classification, and solid waste treatment are all effective ways to reduce carbon emissions.

Conclusion

Reducing CO_2 emissions is an urgent need for China to reach peak carbon emissions. Accurate prediction of CO_2 emissions will help China to formulate relevant policies and implement feasible measures to reduce CO_2 emissions. Several factors affect CO_2 emissions, among which population growth,

economic expansion, urbanization, transportation, energy, and industrial structure have non-negligible correlations with CO_2 emissions. In this context, this study proposes a novel grey prediction model. By considering the influence of various aspects, two numerical cases of CO_2 emissions per capita are selected for modeling in this study, and the proposed model considers the influence of various aspects such as GDP per capita and urbanization rate, to improve the accuracy of prediction.

The theoretical framework of this study incorporates a fractional order operator in the NGM (1, N) model to enhance the impact of recent information and an optimized background value coefficient to improve prediction accuracy. Thus, the FNBGM (1, N, r) model is proposed. In addition, the WOA algorithm is utilized instead of the traditional technique of selecting coefficients to optimize the fractional order and background value coefficient. In addition, the least squares method is used to calculate the model parameters and derive the time response equation as a reliable tool for predicting future trends.

The empirical analysis of this study demonstrated the validity and accuracy of the proposed FBNGM (1, N, r) model, which is used to model the World Bank's CO_2 emissions per capita data for the years 1990 to 2020, as well as the CO_2 emissions per capita data from energy calculated from the China Statistical Yearbook's energy data for the years 1990 to 2022. In addition, this study conducts a comparative analysis to verify the validity of the FBNGM (1, N, r) model proposed in this paper. Specifically, univariate grey prediction models NGM (1, 1), FNGM (1, 1), FBNGM (1, 1), multivariate grey prediction models NGM (1, N) and FNGM (1, N) models and non-grey prediction models MLR, SVR, and BPNN were developed in this study using two numerical cases. On the training and test sets, using RMSE, MSE, APE, and MAPE to compare the accuracy of these models with the FBNGM (1, N, r) model. Based on the results of the comparative analysis, it can be concluded that the FBNGM (1, N, r) model proposed in this study has the highest accuracy compared to other models. The MAPE values for the training and test sets of case 1 are 1.29% and 0.61%, respectively. Meanwhile, the MAPE values for the training and test sets of case 2 are 1.04% and 1.38%, respectively. Based on the evaluation criteria listed in Table 3, it is evident that the proposed model performs well on both the training and test sets in the two specific cases studied.

Furthermore, this study utilizes the high-accuracy model proposed to predict future CO_2 emissions per capita for the two numerical cases. The results indicate that CO_2 emissions per capita from the energy sector are expected to continue decreasing from 2023 onwards, while the combined CO_2 emissions per capita will continue to increase. Based on the projections of this study, China has now achieved initial results in energy structure transformation, i.e., reducing fossil energy consumption and increasing clean energy consumption, and will need to further strengthen its carbon reduction efforts in transportation, industrial production, and other areas in the future. In addition, this study proposes a series of recommendations aimed at reducing CO_2 emissions per capita.

The results of the numerical case study convincingly demonstrate that the FBNGM (1, N, r) model proposed in this study accurately predicts CO_2 emissions per capita. However, there is still considerable work to be done to conduct a more comprehensive analysis of the characteristics of CO_2 emissions per capita. In future studies, it would be beneficial to investigate the differences in CO_2 emissions among countries with varying income levels and development situations. Moreover, the model can be enhanced in terms of its structure and other relevant aspects to attain an even higher level of accuracy.

Author contribution Yan Xu: supervision, writing, review, and editing. Tong Lin: conceptualization, software, writing — original draft. Pei Du: conceptualization, methodology, supervision, writing, review, and editing. Jianzhou Wang: validation, formal analysis.

Funding This work was partly supported by the National Key Research and Development Program of China (No. 2023YFB3308903), the Humanities and Social Sciences of Ministry of Education Planning Fund (No. 22YJA910004 and No. 22YJCZH028), the Soft Science Project of Shaanxi Province Fund (No. 2022KRM093), and the Fundamental Research Funds for the Central Universities Fund (No. SK2022040).

Data Availability The datasets used and/or analyzed during the current study are available from the corresponding author on reasonable request.

Declarations

Ethics approval Not applicable.

Consent to participate Not applicable.

Consent for publication Manuscript is approved by all authors for publication.

Competing interests The authors declare no competing interests.

References

Ağbulut Ü (2022) Forecasting of transportation-related energy demand and CO2 emissions in Turkey with different machine learning algorithms. Sustain Prod Consum 29:141–157. https://doi.org/10.1016/j.spc.2021.10.001

Aslam B, Hu J, Shahab S, Ahmad A, Saleem M, Shah SSA, ... Hassan M (2021) The nexus of industrialization, GDP per capita and CO2 emission in China. Environ Technol Innov 23:101674. https://doi.org/10.1016/j.eti.2021.101674.

Cai P, Zhang C, Chai J (2023) Forecasting hourly PM2. 5 concentrations based on decomposition-ensemble-reconstruction framework incorporating deep learning algorithms. Data Sci Manag 6(1):46–54. https://doi.org/10.1016/j.dsm.2023.02.002

Chen HB, Pei LL, Zhao YF (2021) Forecasting seasonal variations in electricity consumption and electricity usage efficiency of industrial sectors using a grey modeling approach. Energy 222:119952. https://doi.org/10.1016/j.energy.2021.119952

Chen J, Chen Y, Mao B, Wang X, Peng L (2022a) Key mitigation regions and strategies for CO2 emission reduction in China based on STIRPAT and ARIMA models. Environ Sci Pollut Res 29(34):51537–51553. https://doi.org/10.1007/s11356-022-19126-w

Chen Q, Lai X, Gu H, Tang X, Gao F, Han X, Zheng Y (2022b) Investigating carbon footprint and carbon reduction potential using a cradle-to-cradle LCA approach on lithium-ion batteries for electric vehicles in China. J Clean Prod 369:133342. https://doi.org/10.1016/j.jclepro.2022.133342

Dalla Longa F, Fragkos P, Nogueira LP, van der Zwaan B (2022) System-level effects of increased energy efficiency in global low-carbon scenarios: a model comparison. Comput Ind Eng 167:108029. https://doi.org/10.1016/j.cie.2022.108029

Delanoë P, Tchuente D, Colin G (2023) Method and evaluations of the effective gain of artificial intelligence models for reducing CO2 emissions. J Environ Manag 331:117261. https://doi.org/10.1016/j.jenvman.2023.117261

Ding S, Zhang H (2023) Forecasting Chinese provincial CO2 emissions: a universal and robust new-information-based grey model. Energy Econ 121:106685. https://doi.org/10.1016/j.eneco.2023.106685

Ding S, Xu N, Ye J, Zhou W, Zhang X (2020) Estimating Chinese energy-related CO2 emissions by employing a novel discrete grey prediction model. J Clean Prod 259:120793. https://doi.org/10.1016/j.jclepro.2020.120793

Ding S, Hu J, Lin Q (2023a) Accurate forecasts and comparative analysis of Chinese CO2 emissions using a superior time-delay grey model. Energy Econ 126:107013. https://doi.org/10.1016/j.eneco.2023.107013

Ding Q, Xiao X, Kong D (2023b) Estimating energy-related CO2 emissions using a novel multivariable fuzzy grey model with time-delay and interaction effect characteristics. Energy 263:126005. https://doi.org/10.1016/j.energy.2022.126005

Ehigiamusoe KU, Dogan E (2022) The role of interaction effect between renewable energy consumption and real income in carbon emissions: evidence from low-income countries. Renew Sustain Energy Rev 154:111883. https://doi.org/10.1016/j.rser.2021.111883

Gao M, Yang H, Xiao Q, Goh M (2022) A novel method for carbon emission forecasting based on Gompertz's law and fractional grey model: evidence from American industrial sector. Renew Energy 181:803–819. https://doi.org/10.1016/j.renene.2021.09.072

Gyamfi BA, Adedoyin FF, Bein MA, Bekun FV, Agozie DQ (2021) The anthropogenic consequences of energy consumption in E7 economies: juxtaposing roles of renewable, coal, nuclear, oil and gas energy: evidence from panel quantile method. J Clean Prod 295:126373. https://doi.org/10.1016/j.jclepro.2021.126373

He L, Wang B, Xu W, Cui Q, Chen H (2022) Could China's long-term low-carbon energy transformation achieve the double dividend effect for the economy and environment?. Environ Sci Pollut Res 1–17. https://doi.org/10.1007/s11356-021-17202-1.

Huang R, Zhang S, Wang P (2022a) Key areas and pathways for carbon emissions reduction in Beijing for the "Dual Carbon" targets. Energy Policy 164:112873. https://doi.org/10.1016/j.enpol.2022.112873

Huang Z, Dong H, Jia S (2022b) Equilibrium pricing for carbon emission in response to the target of carbon emission peaking. Energy Econ 112:106160. https://doi.org/10.1016/j.eneco.2022.106160

Huo W, Zaman BU, Zulfiqar M, Kocak E, Shehzad K (2023) How do environmental technologies affect environmental degradation? Analyzing the direct and indirect impact of financial innovations and economic globalization. Environ Technol Innov 29:102973. https://doi.org/10.1016/j.eti.2022.102973

Jian L, Sohail MT, Ullah S, Majeed MT (2021) Examining the role of non-economic factors in energy consumption and CO2 emissions in China: policy options for the green economy. Environ Sci Pollut Res 28:67667–67676. https://doi.org/10.1007/s11356-021-15359-3. (2021)

Jiang T, Yu Y, Yang B (2022) Understanding the carbon emissions status and emissions reduction effect of China's transportation industry: dual perspectives of the early and late stages of the economic "new normal." Environ Sci Pollut Res 29(19):28661–28674. https://doi.org/10.1007/s11356-021-18449-4

Karakurt I, Aydin G (2023) Development of regression models to forecast the CO2 emissions from fossil fuels in the BRICS and MINT countries. Energy 263:125650. https://doi.org/10.1016/j.energy.2022.125650

Kassouri Y, Bilgili F, Kuşkaya S (2022) A wavelet-based model of world oil shocks interaction with CO2 emissions in the US. Environ Sci Policy 127:280–292. https://doi.org/10.1016/j.envsci.2021.10.020

Kong F, Song J, Yang Z (2022) A novel short-term carbon emission prediction model based on secondary decomposition method and long short-term memory network. Environ Sci Pollut Res 29(43):64983–64998. https://doi.org/10.1007/s11356-022-20393-w

Li B, Haneklaus N (2021) The role of renewable energy, fossil fuel consumption, urbanization and economic growth on CO2 emissions in China. Energy Rep 7:783–791. https://doi.org/10.1016/j.egyr.2021.09.194

Li L, Hong X, Wang J (2020) Evaluating the impact of clean energy consumption and factor allocation on China's air pollution: a spatial econometric approach. Energy 195:116842. https://doi.org/10.1016/j.energy.2019.116842

Li W, Elheddad M, Doytch N (2021a) The impact of innovation on environmental quality: Evidence for the non-linear relationship of patents and CO2 emissions in China. J Environ Manag 292:112781. https://doi.org/10.1016/j.jenvman.2021.112781. (ISSN 0301-4797)

Li Y, Yang X, Ran Q, Wu H, Irfan M, Ahmad M (2021b) Energy structure, digital economy, and carbon emissions: evidence from China. Environ Sci Pollut Res 28:64606–64629. https://doi.org/10.1007/s11356-021-15304-4

Li Y, Zhang C, Li S, Usman A (2022) Energy efficiency and green innovation and its asymmetric impact on CO2 emission in China: a new perspective. Environ Sci Pollut Res 29(31):47810–47817. https://doi.org/10.1007/s11356-022-19161-7

Lin B, Zhu J (2019) Determinants of renewable energy technological innovation in China under CO2 emissions constraint. J Environ Manag 247:662–671. https://doi.org/10.1016/j.jenvman.2019.06.121

Liu S, Forrest J, Yang Y (2012) A brief introduction to grey systems theory. Grey Syst: Theory and Application 2(2):89–104. https://doi.org/10.1108/20439371211260081

Liu Z, Deng Z, Davis SJ, Giron C, Ciais P (2022) Monitoring global carbon emissions in 2021. Nat Rev Earth Environ 3(4):217–219. https://doi.org/10.1038/s43017-022-00285-w

Liu SF, Deng JL (2000) The range suitable for GM (1, 1). Syst Eng Theory Pract 20(5):121–124

Luo G, Baležentis T, Zeng S (2023) Per capita CO2 emission inequality of China's urban and rural residential energy consumption: a Kaya-Theil decomposition. J Environ Manag 331:117265. https://doi.org/10.1016/j.jenvman.2023.117265

Meng M, Niu D (2011) Modeling CO2 emissions from fossil fuel combustion using the logistic equation. Energy 36(5):3355–3359. https://doi.org/10.1016/j.energy.2011.03.032

Mirjalili S, Lewis A (2016) The whale optimization algorithm. Adv Eng Softw 95:51–67. https://doi.org/10.1016/j.advengsoft.2016.01.008

Mohsin M, Abbas Q, Zhang J, Ikram M, Iqbal N (2019) Integrated effect of energy consumption, economic development, and population growth on CO 2 based environmental degradation: a case of transport sector. Environ Sci Pollut Res 26:32824–32835. https://doi.org/10.1007/s11356-019-06372-8

Mohsin M, Naseem S, Sarfraz M, Azam T (2022) Assessing the effects of fuel energy consumption, foreign direct investment and GDP on CO2 emission: new data science evidence from Europe & Central Asia. Fuel 314:123098. https://doi.org/10.1016/j.fuel.2021.123098

Peng J, Huang X, Zhong T, Zhao Y (2011) Decoupling analysis of economic growth and energy carbon emissions in China. Resour Sci 33(4):626–633

Ren F, Long D (2021) Carbon emission forecasting and scenario analysis in Guangdong Province based on optimized Fast Learning Network. J Clean Prod 317:128408. https://doi.org/10.1016/j.jclepro.2021.128408

Shan Y, Huang Q, Guan D, Hubacek K (2020) China CO2 emission accounts 2016–2017. Sci Data 7(1):54. https://doi.org/10.6084/m9.figshare.11793816

Tien TL (2012) A research on the grey prediction model GM (1, n). Appl Math Comput 218(9):4903–4916. https://doi.org/10.1016/j.amc.2011.10.055

Umar M, Xu Y, Mirza SS (2021) The impact of Covid-19 on Gig economy. Econ Res -Ekonomska Istraživanja 34(1):2284–2296. https://doi.org/10.1080/1331677X.2020.1862688

Wan G, Li X, Yin K, Zhao Y (2022) Forecasting carbon emissions from energy consumption in Guangdong Province, China with a novel grey multivariate model. Environ Sci Pollut Res 29(39):59534–59546. https://doi.org/10.1007/s11356-022-19805-8

Wang K, Wu M, Sun Y, Shi X, Sun A, Zhang P (2019) Resource abundance, industrial structure, and regional carbon emissions efficiency in China. Resour Policy 60:203–214. https://doi.org/10.1016/j.resourpol.2019.01.001

Wang R, Mirza N, Vasbieva DG, Abbas Q, Xiong D (2020) The nexus of carbon emissions, financial development, renewable energy consumption, and technological innovation: what should be the priorities in light of COP 21 Agreements? J Environ Manag 271:111027. https://doi.org/10.1016/j.jenvman.2020.111027

Wang Y, Fang X, Yin S, Chen W (2021) Low-carbon development quality of cities in China: evaluation and obstacle analysis. Sustain Cities Soc 64:102553. https://doi.org/10.1016/j.scs.2020.102553

Wei W, Xin-gang Z, Wenjie L, Shuran H (2023) The sustainable development of a low-carbon system using a system dynamics model: a case study of China. J Renew Sustain Energy 15(1). https://doi.org/10.1063/5.0130437.

Weng F, Chen Y, Wang Z, Hou M, Luo J, Tian Z (2020) Gold price forecasting research based on an improved online extreme learning machine algorithm. J Ambient Intell Humaniz Comput 11:4101–4111. https://doi.org/10.1007/s12652-020-01682-z

Weng F, Zhu J, Yang C, Gao W, Zhang H (2022) Analysis of financial pressure impacts on the health care industry with an explainable machine learning method: China versus the USA. Expert Syst Appl 210:118482. https://doi.org/10.1016/j.eswa.2022.118482

Wu Y, Xu B (2022) When will China's carbon emissions peak? Evidence from judgment criteria and emissions reduction paths. Energy Rep 8:8722–8735. https://doi.org/10.1016/j.egyr.2022.06.069

Wu L, Liu S, Liu D, Fang Z, Xu H (2015) Modelling and forecasting CO2 emissions in the BRICS (Brazil, Russia, India, China, and South Africa) countries using a novel multi-variable grey model. Energy 79:489–495. https://doi.org/10.1016/j.energy.2014.11.052. (ISSN 0360-5442)

Wu W, Ma X, Zhang Y, Li W, Wang Y (2020) A novel conformable fractional non-homogeneous grey model for forecasting carbon dioxide emissions of BRICS countries. Sci Total Environ 707:135447. https://doi.org/10.1016/j.scitotenv.2019.135447

Xiaomin G, Chuanglin F (2023) How does urbanization affect energy carbon emissions under the background of carbon neutrality? J Environ Manag 327:116878. https://doi.org/10.1016/j.jenvman.2022.116878

Xie W, Wu WZ, Liu C, Zhang T, Dong Z (2021) Forecasting fuel combustion-related CO 2 emissions by a novel continuous fractional nonlinear grey Bernoulli model with grey wolf optimizer. Environ Sci Pollut Res 28:38128–38144. https://doi.org/10.1007/s11356-021-12736-w

Xin-Gang Z, Wei W, Jieying W (2022) The policy effects of demand-pull and technology-push on the diffusion of wind power: a scenario analysis based on system dynamics approach. Energy 261:125224. https://doi.org/10.1016/j.energy.2022.125224

Xu G, Schwarz P, Yang H (2019) Determining China's CO2 emissions peak with a dynamic nonlinear artificial neural network approach and scenario analysis. Energy Policy 128:752–762. https://doi.org/10.1016/j.enpol.2019.01.058

Yang C, Zhang H, Weng F (2024) Effects of COVID-19 vaccination programs on EU carbon price forecasts: evidence from explainable machine learning. Int Rev Financ Anal 91:102953. https://doi.org/10.1016/j.irfa.2023.102953

Ye L, Xie N, Hu A (2021) A novel time-delay multivariate grey model for impact analysis of CO2 emissions from China's transportation sectors. Appl Math Model 91:493–507. https://doi.org/10.1016/j.apm.2020.09.045

Ye L, Yang D, Dang Y, Wang J (2022) An enhanced multivariable dynamic time-delay discrete grey forecasting model for predicting China's carbon emissions. Energy 249:123681. https://doi.org/10.1016/j.energy.2022.123681

Yu L, Ma X, Wu W, Xiang X, Wang Y, Zeng B (2021) Application of a novel time-delayed power-driven grey model to forecast photovoltaic power generation in the Asia-Pacific region. Sustain Energy Technol Assess 44:100968. https://doi.org/10.1016/j.seta.2020.100968

Zeng B, Li H (2021) Prediction of coalbed methane production in China based on an optimized grey system model. Energy Fuels 35(5):4333–4344. https://doi.org/10.1021/acs.energyfuels.0c04195

Zeng B, Luo C, Liu S, Li C (2016) A novel multi-variable grey forecasting model and its application in forecasting the amount of motor vehicles in Beijing. Comput Ind Eng 101:479–489. https://doi.org/10.1016/j.cie.2016.10.009

Zeraibi A, Ahmed Z, Shehzad K, Murshed M, Nathaniel SP, Mahmood H (2022) Revisiting the EKC hypothesis by assessing the complementarities between fiscal, monetary, and environmental development policies in China. Environ Sci Pollut Res 1–16. https://doi.org/10.1007/s11356-021-17288-7

Zhang F, Deng X, Phillips F, Fang C, Wang C (2020) Impacts of industrial structure and technical progress on carbon emission intensity: evidence from 281 cities in China. Technol Forecast Soc Chang 154:119949. https://doi.org/10.1016/j.techfore.2020.119949

Zhao E, Sun S, Wang S (2022) New developments in wind energy forecasting with artificial intelligence and big data: a scientometric insight. Data Sci Manag 5(2):84–95. https://doi.org/10.1016/j.dsm.2022.05.002

Zhou W, Wu X, Ding S, Pan J (2020) Application of a novel discrete grey model for forecasting natural gas consumption: a case study of Jiangsu Province in China. Energy 200:117443. https://doi.org/10.1016/j.energy.2020.117443